A Study of Formation Mechanism of Stationary Line-shaped Precipitation Systems in Japan during the Warm Season

(暖候期の日本における線状降水帯の形成メカニズムに関する研究)

MIN, Kyeongseok

(閔　庚夕)

A dissertation for the degree of Doctor of Science

Department of Earth and Environmental Sciences,

Graduate School of Environmental Studies, Nagoya University

(名古屋大学大学院環境学研究科地球環境科学専攻学位論文　博士（理学）)

2021

Abstract

A stationary line-shaped precipitation system (SLPS), which is one of mesoscale convective systems (MCSs), is a typical heavy-rain-producing weather system formed during warm seasons in Japan. Since an SLPS prediction is difficult, it is important that the formation mechanism of SLPSs is clarified and their conceptual model is established. In this research, two SLPS cases were studied, using observational data and high-resolution numerical experiments: 1 September 2015 over the Kinki district and 7 July 2018 over highlands in Tokai district, respectively.

The first half of the study investigated the SLPS event that occurred on 1 September 2015 over the Kinki district. Although the Kinki district, western Japan, is known as a frequent occurrence region for SLPSs, their formation mechanisms in the region have not been sufficiently clarified yet because of their complex formation processes. Numerical sensitivity experiments were also performed with regard to the topography and initial time. During the SLPS event, the observational data showed that the relative humidity at lower levels was high. The southwesterly was dominant at middle levels over the Kinki district during the formation of the SLPS. The formation of the SLPS was associated with neither a mesoscale low-pressure system nor a synoptic-scale cold front, demonstrating that these were not necessary conditions for the formation of the SLPS. In the numerical experiments, the SLPS was formed in a low-level convergence zone of the westerly with the warm and humid south-southwesterly from

the Kii Channel. New convective cells generated over the north of Awaji Island and are propagated northeastward by the middle-level southwesterly. This cell formation process was repeated and resulted in the formation of the SLPS. The sensitivity experiments for the orography around the occurrence area of the SLPS indicated that the orography was not an essential factor for the formation of the SLPS in this event. The orography can alter the location of the SLPS.

The latter part of this study investigates the orographic effect for the formation of SLPS over the highlands in the Tokai district, central Japan. In July 2018, a heavy rainfall event occurred in the Tokai district in association with the stagnated Baiu front. The total precipitation amount was 1214.5 mm at a rain-gauge point during the heavy rainfall event and roughly a half (623 mm) of the amount was recorded from 6 to 7 July 2018. When the three-hour precipitation amount more than 80 mm was observed from 2300 UTC 6 to 0300 UTC 7 July, an SLPS formed over the highlands in the Tokai district. To investigate the orographic effect for the formation of the SLPS, this study examined observed data, the simulation and sensitivity experiments. The simulation showed that a warm and humid southerly was present to the south of the Baiu front. The humid air was lifted by the windward slopes of the highlands and convective cells developed. They were moved with developing to the northeast by the middle-level southwesterly. During the SLPS formation, secondary convective lines were formed on the southeast side of SLPS. This process was maintained due to environmental

conditions such as stagnation of the Baiu front. In the sensitivity experiments of the orography of the highlands, this study found that the total precipitation amounts of the SLPS were less than a half of that of the simulation experiment. This indicates that the topography of the highlands plays an important role for the formation of the SLPS. The topography triggered and reinforced convective cells, which results in the formation and rainfall enhancement of SLPS.

In summary, in the SLPS case on 7 July 2018, the formation of the SLPS is determined by the orography of the highlands. In the SLPS case on 1 September 2015, the orographic effect was not essential for the formation mechanism. It is expected that more studies of SLPS cases with these complex characteristics are made for further understanding and develop conceptual models in the future for more accurately predicting SLPS during the warm seasons.

CONTENTS

1. Introduction

1.1 Stationary line-shaped precipitation systems

During warm seasons (May—September) in East Asia, heavy rainfall events are occasionally caused by various meteorological phenomena such as typhoons, Baiu front (also known as the Changma-front in Korea and the Meiyu-front in Taiwan and China), extratropical cyclones with fronts, and mesoscale convective systems (MCSs) (Sun and Lee 2002; Wang and Chen 2008; Tsuguti and Kato 2014b). MCSs in midlatitudes have a horizontal scale of over 100 km, and their lifetime is from several hours to several days (Houze 2004). In addition, disasters were frequently caused by heavy rainfall of MCSs. They may be linear or circular in shape and have a very complex formation and maintenance mechanism (Lin 2007). Also, they formed in several different patterns, line-shaped precipitation systems produced heavy rainfall during warm seasons in cases without typhoons (Ogura 1991; Tsuguti and Kato 2014a).

When a line-shaped precipitation system stagnates at almost the same location, a large rainfall is taken there. Unuma and Takemi (2016a) found that a slower-moving convective cluster has higher precipitation intensity than a faster-moving convective cluster using weather radars and upper-air sounding data during the warm season. Kato (2020) defined a *Senjo-Kousuitai* as an MCS which consists of several convective cells or clusters aligned linearly with a width of 20–50 km and a length of approximately 50–300 km. Occasionally, these systems remain stationary for several hours. Hirockawa et al. (2020) classified four types of

heavy rainfall areas during warm seasons in Japan; linear-stationary, linear, stationary, and other using weather radar data. They found that approximately 80% of linear-stationary types have a characteristic feature defined by Kato (2020).

In previous studies, for extraction of SLPS, they used total precipitation amounts (Japan Meteorological Agency (JMA) 2018; Kato 2020). In this study, a stationary line-shaped precipitation system (SLPS) referred to a precipitation system defined by Kato (2020).

1.2 SLPS classifications

The patterns of line-shaped MCSs, including those of SLPSs, were classified in previous studies. Bluestein and Jain (1985) studied the squall-line formation processes over Oklahoma, United States, during spring seasons. They classified the formation patterns of linear MCSs into four types; broken-line (BL), back-building (BB), broken-areal, and embedded-areal types. They found that line-shaped MCSs formed under unstable environmental conditions with large convective available potential energy (CAPE). Parker and Johnson (2000), using weather radar observations, proposed three conceptual models of line-shaped MCSs with the stratiform precipitation occurring in the United States; trailing-stratiform, leading-stratiform, and parallel-stratiform. They also found that each type of these line-shaped MCSs was formed in different environments and that these environments influenced the travel speed and duration of the MCSs. Schumacher and Johnson (2005) studied the structure and environmental

properties of SLPSs in the area east of the Rocky Mountains, United States, by using radar data and a numerical model. They proposed a training line/adjoining stratiform as a new type of line-shaped MCS in addition to the BB type. They reported that BB type MCSs depend on small-scale processes such as the storm-scale (2–20 km) or meso-scale (20–several hundred km) processes rather than the large-scale ones and that clarifying their environmental conditions is more difficult than that for other linear MCSs. Gallus et al. (2008) identified convective storms that occurred over the central United States in the warm season of 2002 using the classifications of the above studies (Fig. 1.1). They found that linear-type MCSs had a higher threat of causing severe weather events such as hail, flooding, and tornados than isolated cells or convective clusters.

In Japan, Seko (2010) proposed a back-and-side-building (BSB) type for the SLPS formation, in addition to Squall line and the BB type (Fig. 1.2). From numerical experiments, they confirmed that the type of SLPSs was determined by wind directions at low and middle levels. Under the condition in which the low and middle-level wind directions are almost parallel, BB-type MCSs are formed by the successive formation of convective cells and their leeward movements. In contrast, BSB type MCSs produce a carrot-shaped precipitation area, and the low-level inflow comes from the right-hand side of the middle-level flow. Kato (2020) proposed that the formation mechanism of SLPSs was categorized into two types: BL and BB type.

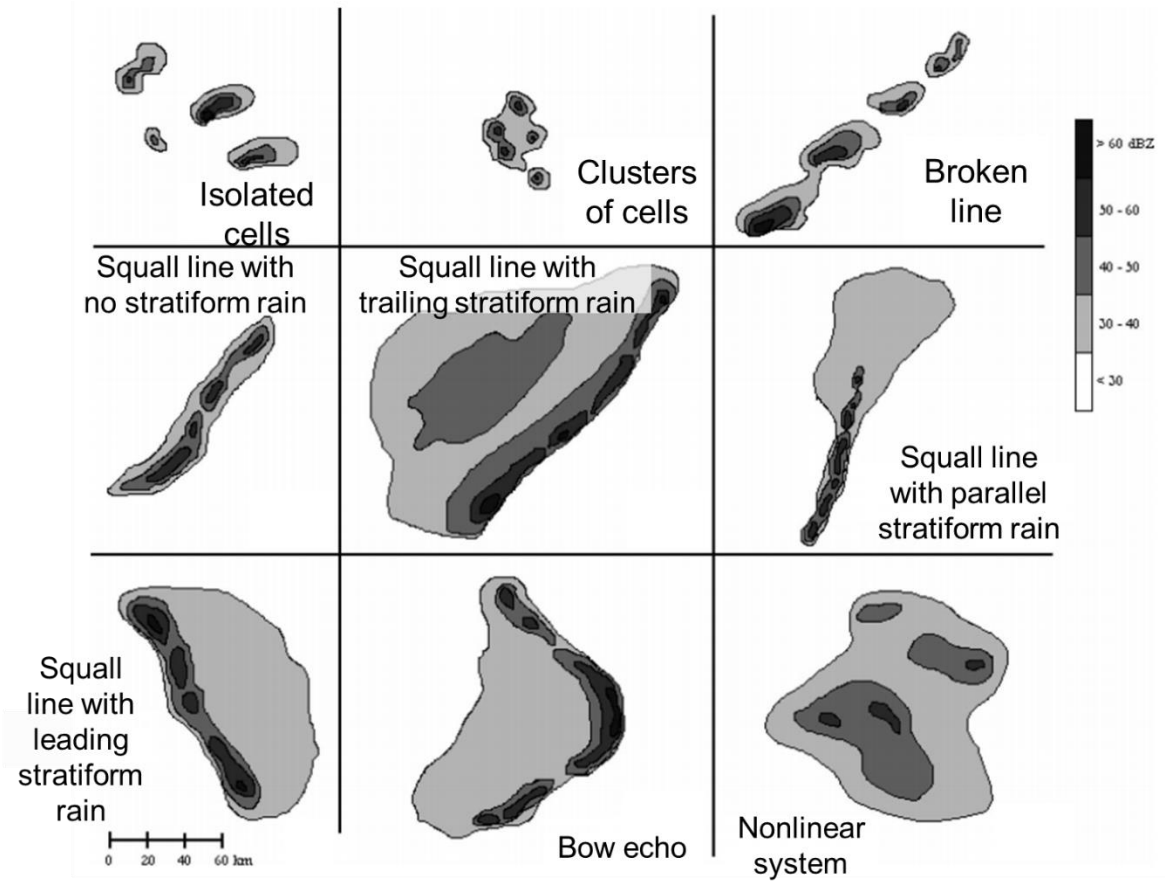

Fig. 1.1. Schematic demonstrating each of the nine storm morphologies used in the classification system in Gallus et al. (2008).

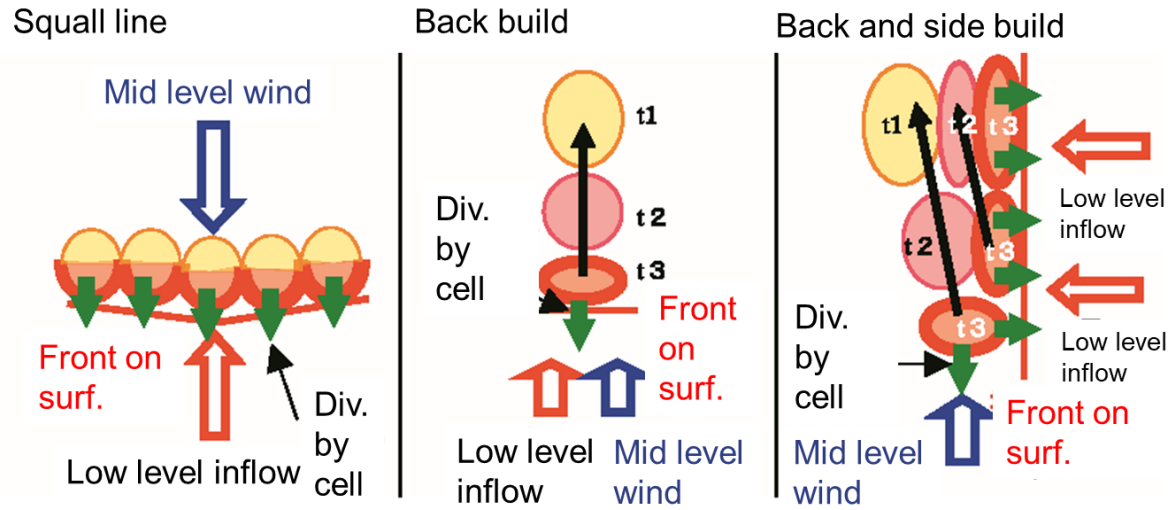

Fig. 1.2. Schematics of the three type morphologies used in the classification in Seko (2010). The older convective cells are denoted by yellow than those of newer convective cells. The black and green arrows indicate the traveling and divergence of convective cells, the red and blue arrows indicate the low-level inflow and middle-level winds, respectively.

1.3 The formation mechanism of SLPSs

In section 1.2, SLPSs were classified into several types by shape. Most of these differences are related to formation mechanisms with different environmental conditions. SLPSs form under complex conditions. Previous studies about SLPS proposed some SLPS formation essential factors, environmental condition and the orographic effect.

SLPSs formed in environments of various weather systems such as the Baiu front, a cold front, and a convergence line in the lower troposphere (Kato 2020). Seko et al. (1999) conducted numerical experiments for the BB formation mechanism of SLPS in eastern Japan during a typhoon approached Japan Island. They suggested essential factors for the formation are the high equivalent potential temperature (EPT) advection from the windward side at the low-level and the vertical wind shear. Kato and Goda (2001) also suggested that an important factor is the near-surface advection of warm air during the Baiu-season. Seko and Nakamura (2003) conducted sensitivity experiments on middle-level humidity and found that the SLPS type was not affected by middle-level humidity. In contrast, Kato (2006) studied the structure of an SLPS that occurred over northern Kyushu, western Japan, in 1999 and found that the humid southwesterly at low levels and the dry westerly at middle levels enhanced convective instability. He also found that the top height of cumulonimbus clouds was controlled by the inflow amounts of dry air at middle levels that suppressed the further development of

cumulonimbus clouds. A large intrusion of middle-level dry air into convective cells decreased their buoyancy owing to evaporative cooling.

As described above studies, for the SLPS which is formed by several environmental factors, Kato (2020) proposed six favorable occurrence conditions for SLPSs; large amount of water vapor flux (FLWV) at low levels, short distances to the level of free convection (dLFC), high relative humidity (RH) at middle levels, large storm-relative environmental helicity (SREH) estimated due to the large vertical wind shear, upward motion of synoptic-scale environment, and the exclusion of warm air advection frequently appearing at 700–800 hPa and inhibiting the development of convection.

In some cases of SLPSs, topography often plays an important role in the formation mechanism. When a humid inflow reaches topography, the low-level air is lifted to form the precipitation system. Orographic lifting and blocking may modify and/or form precipitation systems around the topography (Lin, 2007). Previous studies found the event that the orographic effect was one of the essential factors in SLPS formation (Fig. 1.3). Kurihara et al. (2009) studied an SLPS in Hiroshima, western Japan, when a warm front of an extratropical cyclone passed. Sensitivity experiments of orography were conducted with an elevation height of 0 m around Hiroshima and Shikoku Island, western Japan. They found that the orography affected the inflow of the water vapor on the windward side and SLPS development speed. As

a result, it changed the total precipitation amounts of the SLPS. The orography also influenced the formation of low-level convergence that triggered the SLPS (Takahashi et al. 2019).

Higashi et al. (2010) proposed multiscale factors such as a cold front extending from a meso-α-scale (200–2000 km horizontal scale) cyclone, meso-β-scale (20–200 km horizontal scale) low near Shikoku Island, and meso-γ-scale (2–20 km horizontal scale) lee waves generated by Awaji Island in the Kinki district. Ishihara and Takara (2018) showed a new formation mechanism of SLPSs in the Kinki district, which was not related to a cold front. They highlighted the importance of the warm and humid southerly inflow through the Kii Channel in the lower layers and the topography of Mount Rokko.

In some SLPS cases, the terrain triggers the convective cells in SLPS, such as lifting the air (Yoshizaki et al. 2000). Moritomi et al. (2012) found that the Yoro Mountains with Ibuki-Suzuka mountains in the Tokai district (Fig. 1.4c) convergent low-level humid air and generated a convective cell of SLPS. In addition, on the windward side of SLPS, atmospheric instability was caused by the low-level humid air during the SLPS process. On the other hand, orographic effects for the formation of SLPS are not sufficiently clarified, and an orography hardly affects the formation and maintenance processes of some SLPS cases (Kato and Goda 2001; Tsuguti 2019; Kawano and Kawamura 2020). This indicates the complexity of SLPS formation.

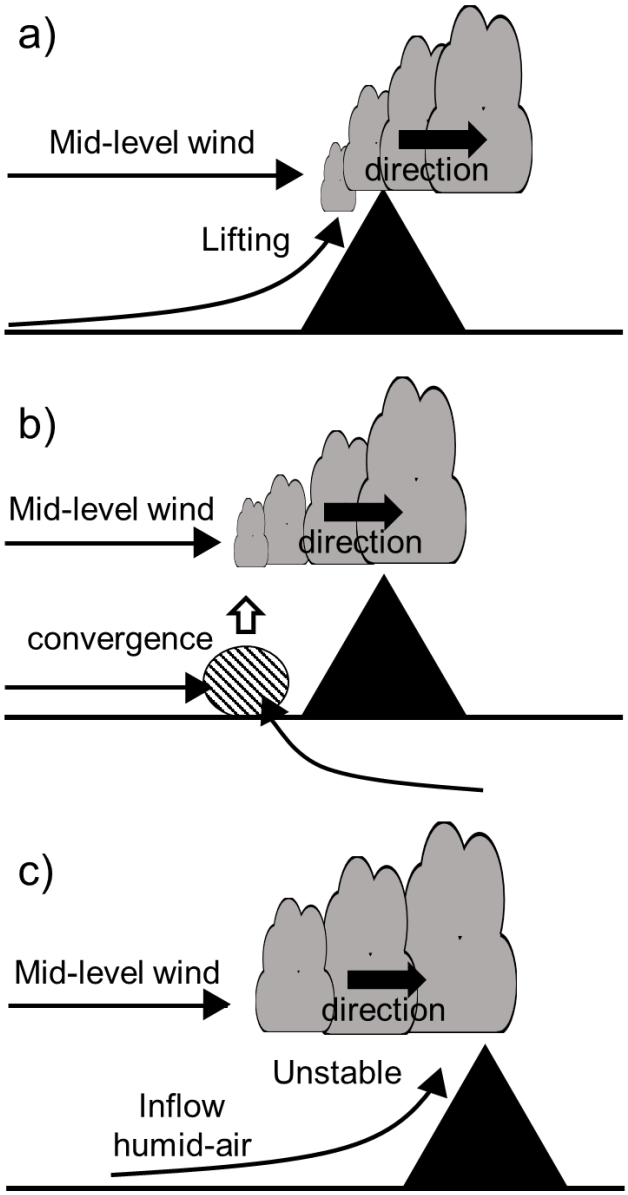

Fig. 1.3 Schematics of the three type morphologies for orographic effect during SLPS. a) The trigger of the convective cell in SLPS such as lifting the air, b) generation of low-level convergence, and c) enhancement of SLPS rainfall by atmospheric instability condition at low level, respectively.

1.4 The objective of this study

As SLPSs in Japan frequently cause disasters, enhancing their forecast accuracy is necessary to reduce disasters (Tsuguti 2016). Toward this goal, it is necessary to investigate the formation mechanisms of several SLPSs in Japan during warm seasons and to explore the influence of various factors such as synoptic conditions, the local convergence, and the topography. The formation mechanism for environmental factors has been conducted through previous studies (Kato 2020). However, it is necessary to study the orographic effect for establishing the SLPS conceptual model.

This study chose two cases of SLPS. First, the SLPS case on 1 September 2015 in the Kinki district was studied (Case1 in Fig. 1.4). In previous studies, SLPSs generated in the Kinki district were affected by the topography surrounding Osaka Bay (Higashi et al. 2010; Ishihara and Takara 2018). Second, the SLPS formed over the highlands in Gifu prefecture on 6 to 7 July 2018 was studied (Case2 in Fig. 1.4). During this period, heavy rainfalls occurred in Japan due to the stagnated Baiu front, and previous studies focused on environmental conditions (JMA 2018; Sueki and Kajikawa 2019). In previous studies, SLPSs generated and maintenance in the Tokai district were affected by the topography of windward side in SLPS (Kato 2002; Moritomi et al. 2012; Takasaki et al 2019). In this study, a detailed analysis of two SLPS events was conducted in the following way;

(1) Observational data including radars and surface weather data were examined to clarify the environmental conditions and characteristics of the SLPS. (2) High-resolution numerical experiments were conducted using the Cloud Resolving Storm Simulator (CReSS) (Tsuboki and Sakakibara, 2002; 2007) to study the SLPS formation mechanisms. (3) Sensitivity experiments were conducted to explore the effects of the orography around the SLPS location.

Section 2 describes the data and the numerical model in this study. In Section 3 and 4, the results of the SLPS events over the Kinki district on 1 September 2015 and over Tokai district on 7 July 2018 are presented. Finally, the study was summarized in section 5.

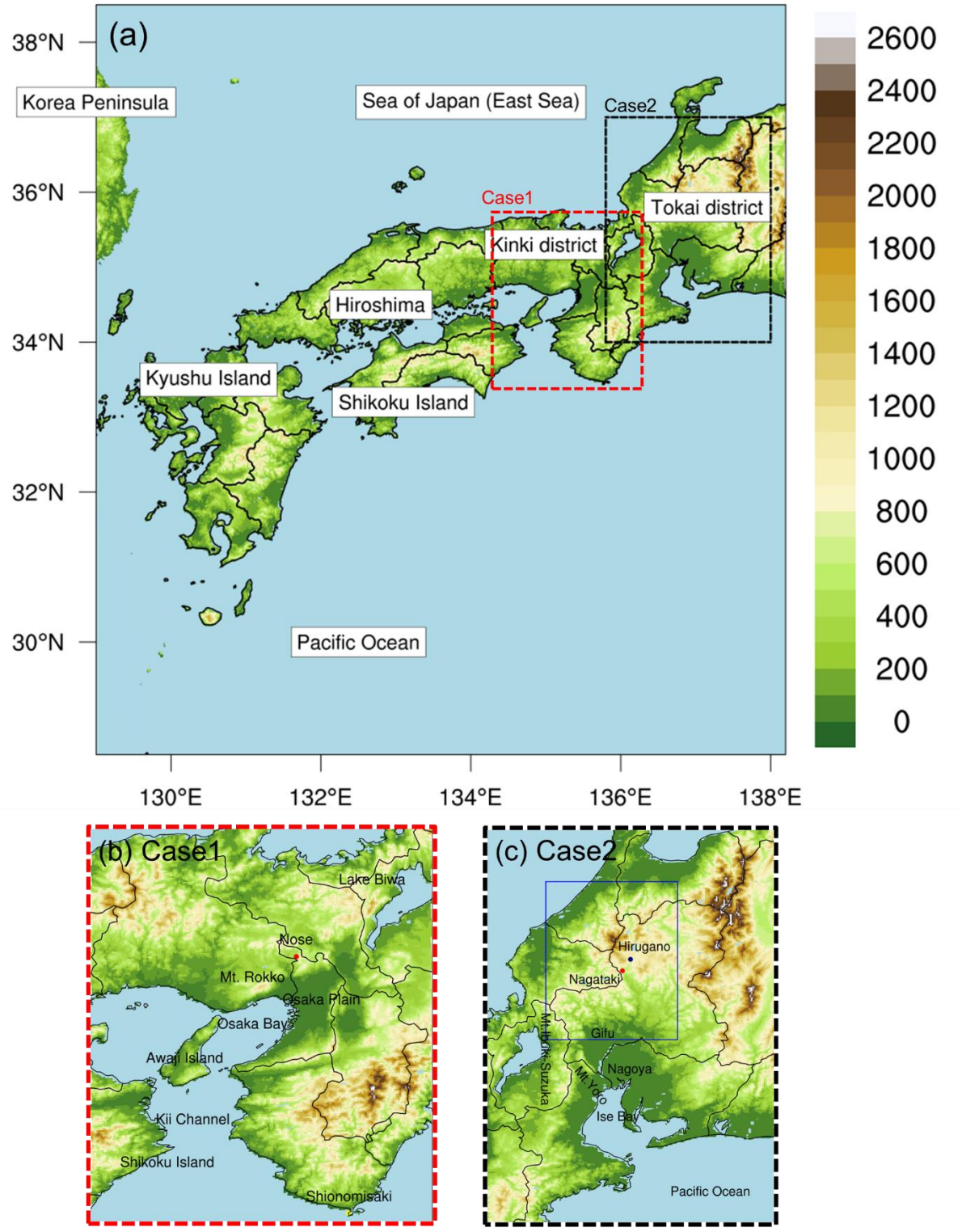

Fig. 1.4 Map of (a) western and central Japan and (b)the Kinki and (c) Tokai district and its neighboring regions. The color scale denotes the height of terrain (m). The red and yellow dots

in (b) indicate the Nose AMeDAS station (34.948° N, 135.455° E) and the Shionomisaki upper observation station (33.450° N, 135.760° E), respectively. The red and blue dots in (c) indicate the Nagataki (35.953° N, 136.832° E) and the Hirugano (36.01° N, 136.893° E) AMeDAS stations, respectively.

2. Data and method

The observational data used in this study were surface data of automated meteorological data acquisition systems (AMeDAS), the weather radar data, and upper-air sounding data, provided by the JMA, on 1 September 2015 and 6 to 7 July 2018. The AMeDAS data include wind speed and direction, rainfall amount, and sunshine duration.

The JMA radar (C-band Doppler, 5.3 GHz) network covering the Japanese islands observes the precipitation intensity every 5 minutes. In this study, to examine the temporal change of the target SLPSs, a constant-altitude plan position indicator (CAPPI) at an altitude of 2 km was used. To understand the synoptic conditions when the SLPS formed, JMA weather charts were used.

The initial and boundary condition in numerical experiments are provided by the JMA mesoscale analysis (JMA-MA, JMA 2013), and the land use data are provided by the United States Geological Survey (USGS) 30-s data. The JMA-MA is produced eight times daily at 0000, 0300, 0600, 0900, 1200, 1500, 1800, and 2100 UTC using a four-dimensional variational technique in which observation data from various systems such as weather radar, satellites, and a ground-based global navigation satellite system are assimilated. The horizontal grid system of the JMA-MA is the Lambert projection with a horizontal resolution of 5 km at 30° N and 60° N with grid numbers of 721 × 577.

The cloud-resolving model, CReSS was used to simulate the structure and time evolution of the SLPS with a high resolution. CReSS is a non-hydrostatic three-dimensional numerical model with a bulk-type cold rain scheme (Lin et al. 1983; Cotton et al. 1986; Murakami 1990; Ikawa and Saito 1991; Murakami et al. 1994). They used Arakawa-C grid and Lorenz grid for the horizontal and vertical grid points, respectively. Smagorinsky one-order closure (1963) or 1.5-order closure of turbulent kinetic energy (TKE) (Deardorff 1980) of parameterizations in the sub-grid scale processes can use in CReSS. Also, they support several types of boundary conditions method; rigid wall, periodic, zero normal-gradient, and wave-radiation types. In this study, all numerical experiments use the 1.5-order closure with TKE scheme and wave-radiating boundary conditions using constant phase velocity. In CReSS, the vertical one-dimension surface (land and sea) processes were considered by simple bulk methods (Louis et al. 1981). They included fluxes of sensible heat and latent heat from the surface to atmosphere, also momentum flux at the surface with friction of the surface. The prognostic variables are three-dimensional velocity components, pressure perturbation, potential temperature perturbation, water vapor mixing ratio, sub-grid scale turbulent kinetic energy, number densities of solid hydrometers (cloud ice, snow, and graupel) and mixing ratios of hydrometeors (cloud water, rain, ice, snow, and graupel). A more detailed description of CReSS is given by Tsuboki and Sakakibara (2002, 2007).

Figure 2.1 shows the computational (solid box) domains in this study. A detailed numerical experiment configuration explained in the result in sections 3 and 4.

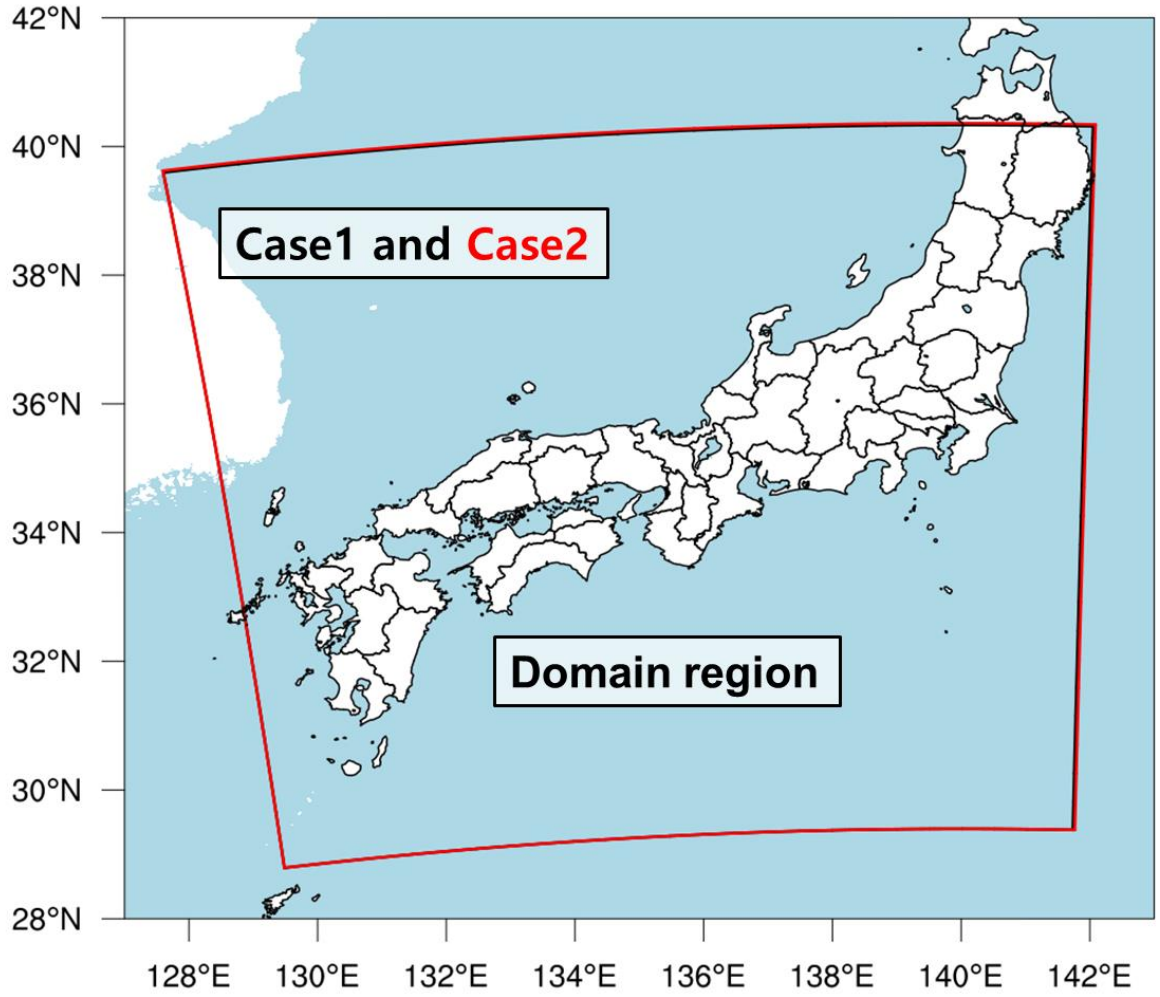

Fig. 2.1 Domain of the simulation experiments for case1 and case2.

3. Case1: SLPS over Kinki district on 1 September 2015

3.1 The environmental conditions over Kinki district on 1 September 2015

Figure 3.1 shows the accumulated amounts of precipitation (mm) and intensity of precipitation (mm h^{-1}) of CAPPIs at a height of 2 km, observed over the Kinki district by the JMA radar network on 1 September 2015. From 0940 UTC to 1200 UTC, the accumulated precipitation amounts distributed in a linear shape from Osaka Bay to Lake Biwa, and the maximum amounts exceeded 50 mm (Fig. 3.1a). According to Unuma and Takemi (2016b), the orientation of the SLPS in this event was frequently observed during warm seasons in Japan. At 0940 UTC, the convective cell C1 formed over Osaka Bay and developed northeastward (Fig. 3.1b). On the upstream (i.e., southwestern) side of cell C1, new cells (C2 and C3) formed and also developed with the northeast movement. This successive convective cell formation process repeated until 1200 UTC (C4, C5, and C6). Consequently, the SLPS formed to extend from the west-southwest to the east-northeast. All of the convective cells formed near the coastline. The formation process of the SLPS was similar to that of the BB type (Bluestein and Jain 1985; Schumacher and Johnson 2005; Gallus et al. 2008). During the period from 1000 UTC to 1200 UTC, the observed total amount of precipitation at the Nose station, which is the closest AMeDAS station to the point with the maximum accumulated amount of precipitation in the SLPS (34.948° N, 135.455° E, Fig. 1.4), was 59.5 mm.

The JMA weather chart at 1200 UTC on 1 September 2015 (Fig. 3.2) shows that an extratropical cyclone with a central pressure of 1006 hPa and a North Pacific high-pressure system sandwiched the Kinki district. Another extratropical cyclone with a central pressure of 1008 hPa was located over the Shandong Peninsula (approximately 36° N, 120° E). The Kinki district was influenced by the southwesterly on the west side of the North Pacific high-pressure system and the westerly on the south side of the extratropical cyclone. This surface pressure pattern was similar to those in the SLPS events studied previously (Seko et al. 2006; Higashi et al. 2010; Meteorological Research Institute (MRI) 2010). However, during the formation of the SLPS, the cold front associated with the extratropical cyclone was located to far west of the Kinki district. The cold front reached the Kinki district when the SLPS had already dissipated at 1800 UTC (not shown). Therefore, in the warm sector between the cold and warm fronts of the extratropical cyclone, the SLPS formed and dissipated. Moreover, when the SLPS formed, there were no abrupt changes in the temperature and wind direction at the AMeDAS observation points in the Osaka Plain (not shown). According to Kato (2020), the present case was categorized to the case of low pressure among the five types of synoptic fields in which SLPSs form. He also showed that the ratio of this type is 12 % of all SLPS cases analyzed in Japan from 1989 to 2015 warm seasons (April—November).

Figure 3.3 shows the upper weather charts at 850 and 500 hPa. The pattern of 850 hPa isohypsis lines was similar to the pattern of surface pressure. In a moist area along dense

isohypse lines, the Kinki district lay. At 850 hPa at Shionomisaki, a wind stronger than 20 knots was observed. This strong wind crossed an 18 °C temperature line at 850 hPa, which resulted in the inflow of warm air to the Kinki district that was shown in Fig. 3.3 by a low dew point depression area. The highly humid air was present over the Kinki district in this case. In the 500 hPa upper weather chart, a trough was present over the Shandong Peninsula, while a low-pressure system located to the north of Japan was not clearly found. In front of the low-pressure trough, the southwesterly with wind speed of approximately 40 knots was present over western Japan.

The upper-air sounding data at Shionomisaki (33.45167° N, 135.7617° E) at 1200 UTC on 1 September 2015 were used to examine the atmospheric condition in the occurrence of the SLPS, such as CAPE, convective inhibition (CIN), and total precipitable water (TPW). Figure 3.4 shows the skew T-log P upper-air diagram at the Shionomisaki station at 1200 UTC 1 September 2015. The lower layer below 846 hPa (1565 m height) was very humid (RH over 80 %) and the wind direction was south-southwesterly. The lifting condensation level (LCL) and level of free convection (LFC) in an air parcel averaged from the surface to 500 m height being lifted adiabatically were low levels of 965.3 hPa (approximately 420 m height) and 928.6 hPa (approximately 760 m height), respectively. The CAPE and CIN estimated by lifting a parcel from a 500 m height were 2382.3 J kg^{-1} and 0.1 J kg^{-1}, respectively. The TPW was 56 mm. These values indicate that the atmosphere was conditionally unstable, and the occurrence

possibility of thunderstorms was high (Schultz et al. 2000). Under the conditions with a large CAPE and a low LFC, convective clouds can easily form by weak forcing at low levels.

These observational data indicate that the atmosphere on the low-level upstream side of the Kinki district was highly conditionally unstable and that weak forcing could easily initiate convective cells. This unstable atmosphere was caused by the low-level inflow of the strong south-southwesterly from the moist air mass over the Pacific Ocean. On the other hand, the SLPS extended to the east-northeast by the southwesterly in the middle troposphere. However, only these observational data are insufficient to explain the atmosphere condition in the present case.

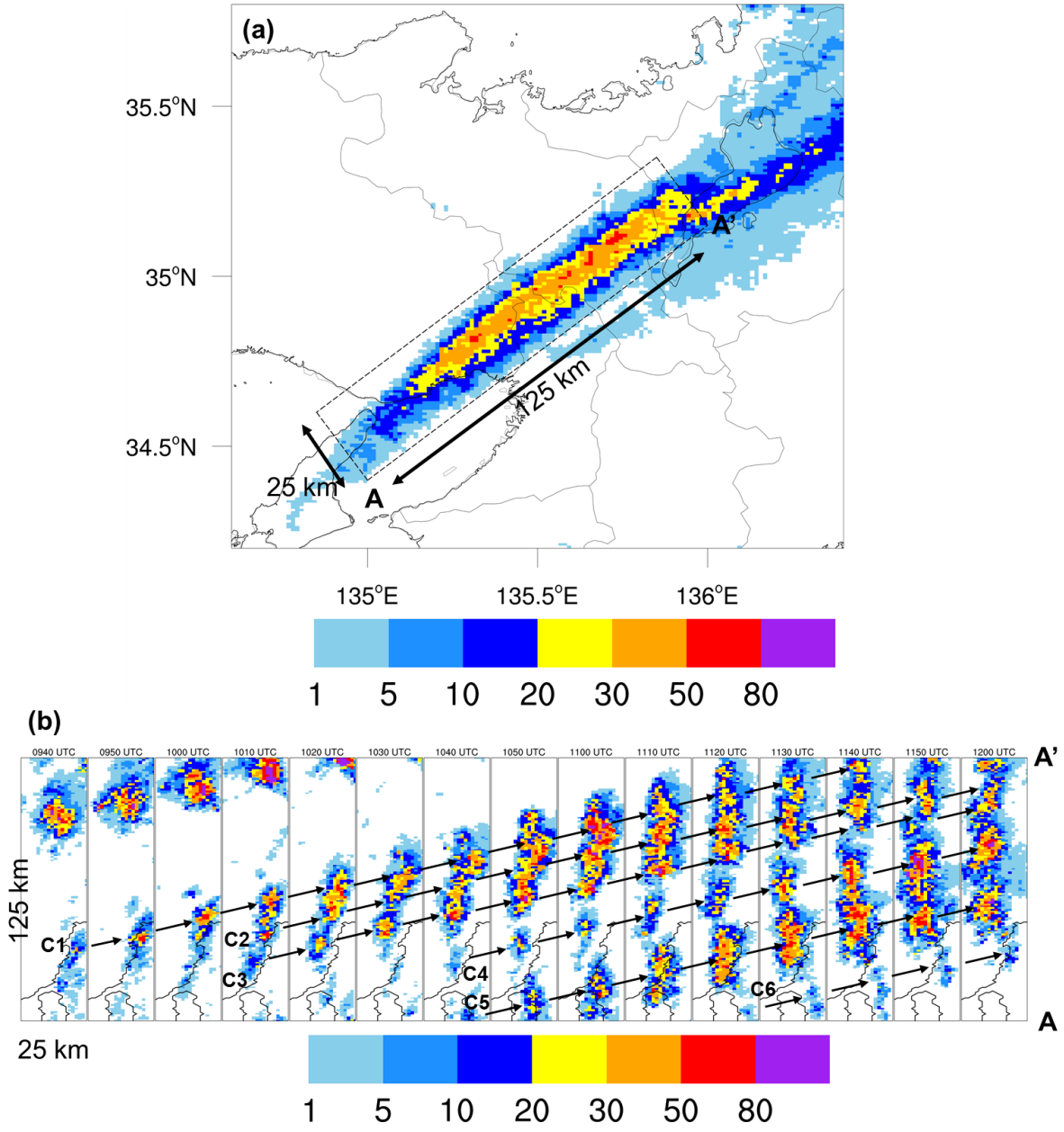

Fig. 3.1 (a) Total precipitation amounts (mm) over the Kinki district from 0940 UTC to 1200 UTC 1 September 2015, obtain from the JMA radar network. The dashed rectangle is the region shown in Fig. 3.1b. (b) CAPPI distributions of precipitation intensity (mm h^{-1}) at a height of 2 km from 0940 UTC to 1200 UTC with a time interval of 10 minutes. C1, C2, C3, C4, C5, and C6 denote individual convective cells, and arrows show their movements.

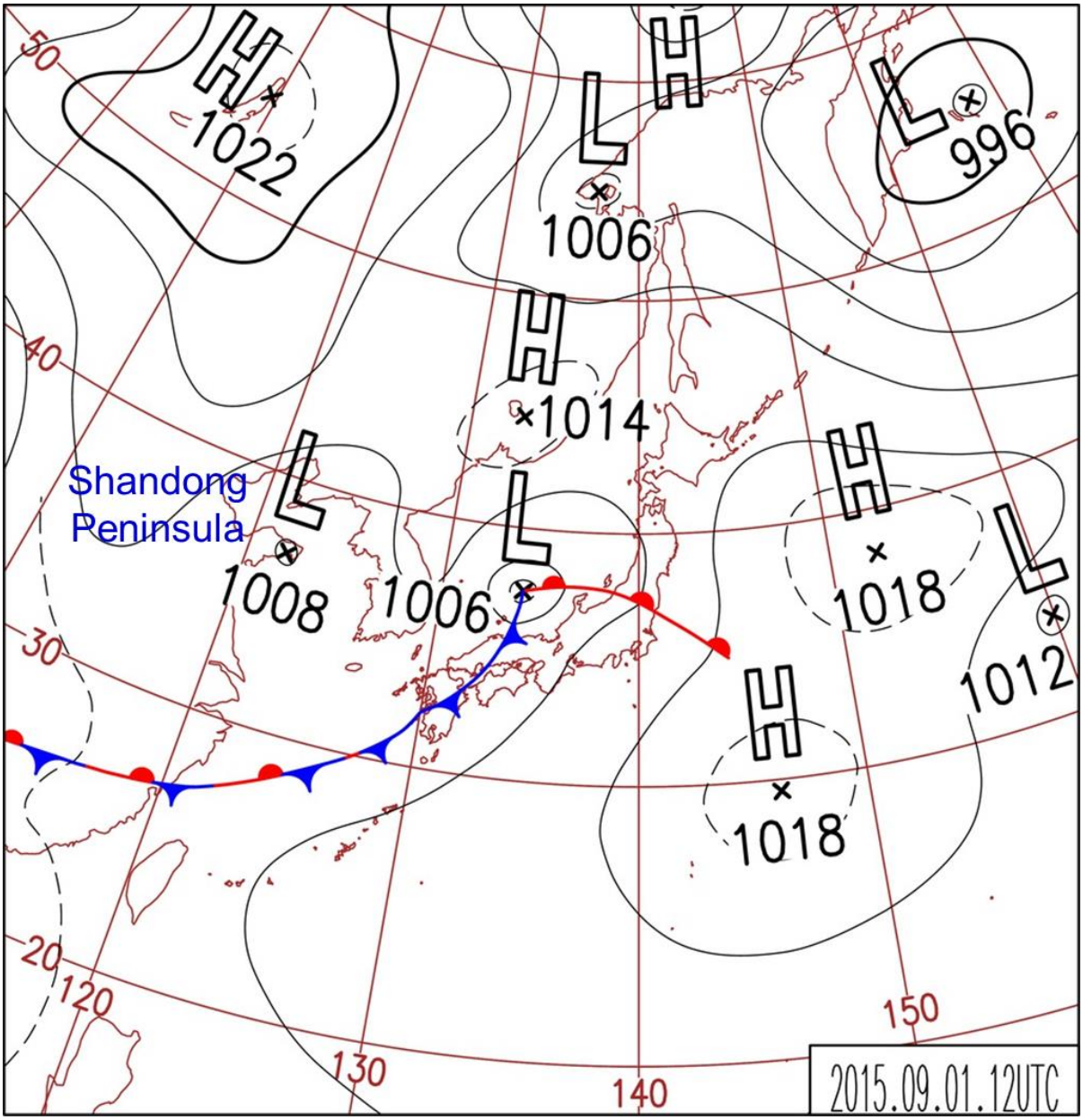

Fig. 3.2 JMA surface weather chart at 1200 UTC on 1 September 2015.

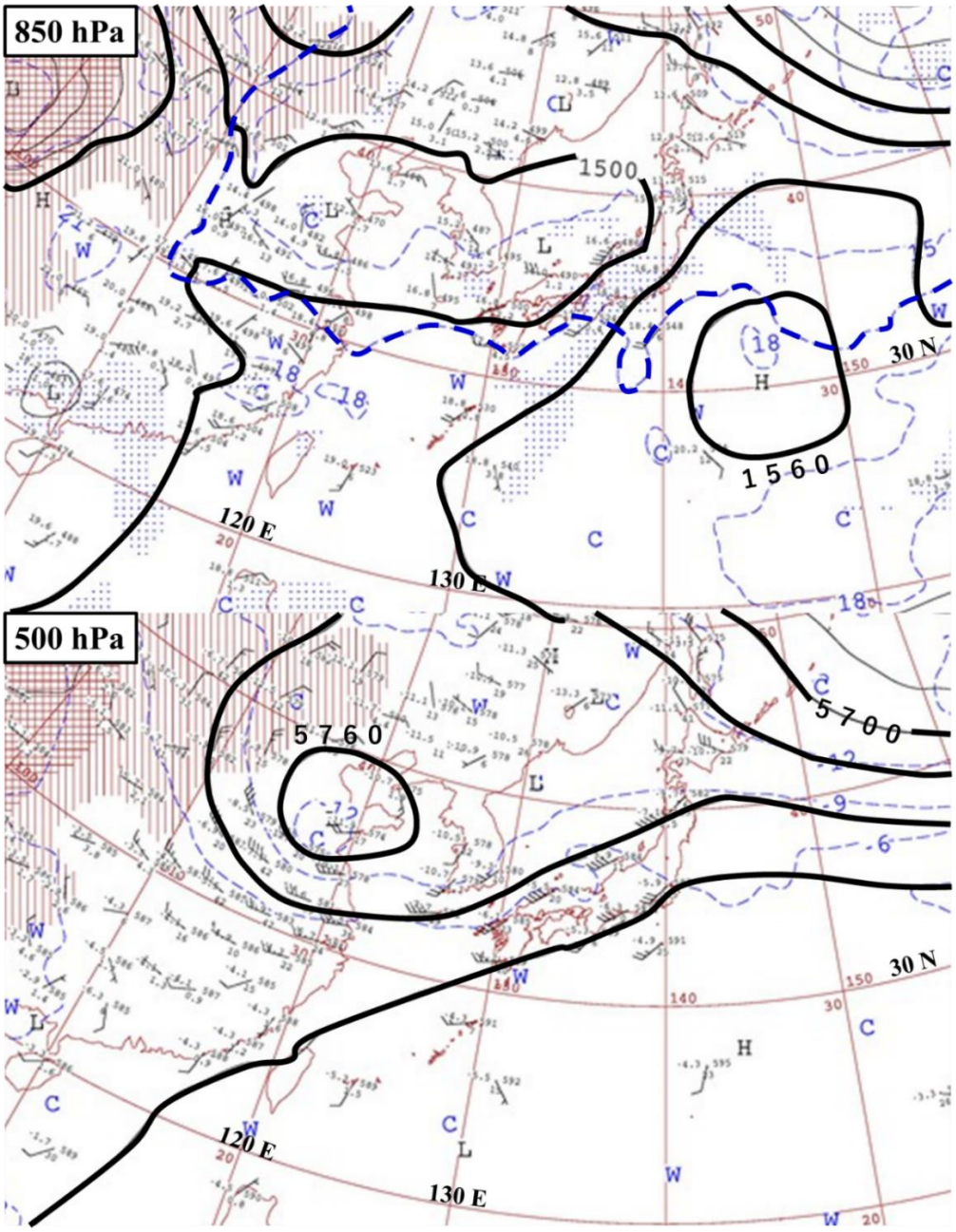

Fig. 3.3 JMA upper weather charts (top: 850 hPa, bottom: 500 hPa) at 1200 UTC 1 September 2015. Bold solid and blue dashed lines denote the geopotential height (m) and temperature (°C), respectively. Dotted regions denote areas where dew point depression (difference between temperature and dew point temperature) is less than 3 °C.

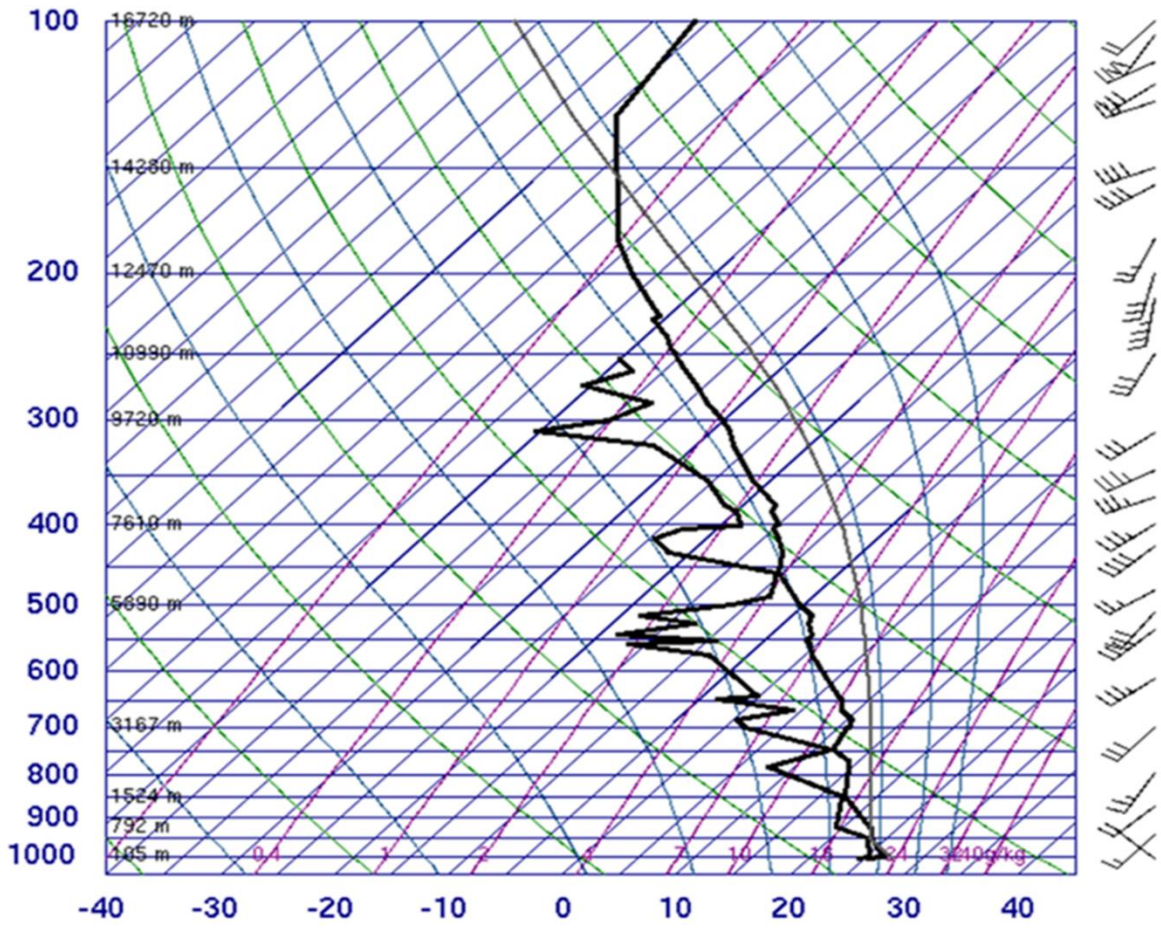

Fig. 3.4 Profiles of temperature and dew point temperature (°C) on skew T-log P diagram observed at the Shionomisaki station at 1200 UTC 1 September 2015. The full and half burbs are wind speeds of 10 knots and 5 knots, respectively.

3.2 Result

3.2.1 Numerical experiment configuration

In numerical experiments on 1 September 2015, the horizontal grid spacing is 1 km, and sixty stretched layers with the model top of 26.6 km were set in a vertical direction. Seven layers are included below 1 km: 25 m, 95 m, 204 m, 346.3 m, 521 m, 726 m, and 958 m. The time step of all experiments is 0.5 seconds. The simulation experiment (CNTL1) and sensitivity experiments for the orography were conducted from 0600 to 1800 UTC on 1 September 2015. Another sensitivity experiment for the environmental conditions was initiated from 0000 UTC on 1 September 2015 (EXP_00, Table 3.1).

To examine the effects of orography and land-use in the Kinki district, sensitivity experiments were conducted in which the land elevation and land-use were changed. In the experiment of ROKKO_100M, the terrain heights of Mount Rokko higher than 100 m were reduced to 100 m. In the experiments of AWAJI_0M and AWAJI_NONE, the terrain heights of Awaji Island were reduced to 0 m and Awaji Island was replaced by sea, respectively. Furthermore, to examine the effect of Shikoku Island, in the experiments of SHIKOKU_NONE and SHIKOKU_0M, the terrain heights of Shikoku Island was also reduced to 0 m and Shikoku Island was replaced by sea, respectively. All of sensitivity experiments were conducted on the orography with the same experimental settings as those in CNTL1.

Table 3.1 The configuration of the numerical experiments to Case1.

Cloud Resolving Storm Simulator Ver. 3.5.0

	CNTL1	EXP_00
Horizontal grid spacing	1 km (1197 x 1197)	
Vertical grid spacing (Top / Bottom height)	450 m (vertically stretched grid, 60 layers) (26620 m / 25 m)	
Time step	0.5 s	
Initial data Boundary data	JMA-MA data (3 Hourly, 5 km)	
Land-use data	USGS 30-s data	
Projection	Lambert Conformal (center at 140° E, secant at 30° and 60° N)	
Sub-grid parameterization	1.5-Order closure with TKE prediction	
Surface processes	Energy and momentum fluxes shortwave and longwave radiation	
Surface model layer	33 layers (land: 0.1 m and sea: 0.3 m)	
Integration period	0600 UTC – 1800 UTC 1 September 2015	0000 UTC 1 – 0000 UTC 2 September 2015

3.2.2 Simulation experiment

To verify the results in CNTL1, the simulated distribution of accumulated two-hour precipitation amounts is compared with that observed by the JMA radar network. Figure 3.5 shows the accumulated precipitation amounts and precipitation intensity in CNTL1 from 1000 UTC to 1200 UTC. Compared with radar observations (Fig. 3.1), the SLPS location and the generation points of convective cells in CNTL1 were slightly shifted to the north (Fig. 3.5), and the linear shape of the SLPS was wider than the observation. The formation of convective cells (Cs1, Cs2, and Cs3 in Fig. 3.5b) that organized the SLPS was delayed by approximately 50 minutes from the radar observations (CNTL1: 1030 UTC, observations: 0940 UTC). In comparison with the radar observations, the precipitation intensity of the convective cells was slightly overestimated. New convective cells (Cs3, Cs4, Cs5, and Cs6) formed on the upstream side of Cs1, Cs2, and Cs3. Although there are some discrepancies between CNTL1 and the observations, the SLPS was well reproduced, particularly the orientation of the SLPS and the cell movements from the west-southwest to the east-northeast. Therefore, the results in CNTL1 were useful in studying the SLPS formation mechanisms.

Figure 3.6 shows the moisture flux convergence (MFC) and horizontal wind vectors over the Kinki district at a height of 521 m from 1000 UTC to 1200 UTC. In this study, the horizontal MFC defined was used by Banacos and Schultz (2005),

$$\mathrm{MFC} = -\left(\frac{\partial \mathrm{qu}}{\partial \mathrm{x}} + \frac{\partial \mathrm{qv}}{\partial \mathrm{y}}\right), \tag{3.1}$$

where u and υ are wind components and q is the specific humidity. A large convergence zone ($> 3 \times 10^{-6}$ g kg^{-1}s^{-1}) was continuously simulated to extend from the northeast part of Shikoku Island to around Mount Rokko through the west coast of Awaji Island from 1000 UTC to 1200 UTC at a height of 521 m. This region corresponded to a horizontal wind shear zone of the westerly and the south-southwesterly. Similar to MRI (2010), in Fig. 3.6e, the westerly was present on the western side of the shear zone. On the other hand, the south-southwesterly was found on the eastern side. Figure 3.7 shows that the westerly (shaded region) developed in the lower layer to the west of Awaji Island (Figs. 3.7a, b, and c dotted circle), associated with the extratropical cyclone that traveled northeastward. Although the low-level convergence zone moved eastward associated with the development of the westerly, the south-southwesterly was maintained to the south of the Kinki district. In the vertical velocity field at a height of 958 m (Fig. 3.8), weak updrafts maintained over the west of Awaji Island and the south of Mount Rokko.

To examine the characteristics of the south-southwesterly and westerly that formed the low-level convergence zone, the EPT distribution with wind vectors at a height of 521 m and two cross-sections along the low-level wind directions are shown by Fig. 3.9. In this study, the EPT θ_e was used defined by Bolton (1980),

$$\theta_e = \theta_L exp\left[\left(\frac{3036}{T_L} - 1.78\right) r(1 + 0.448r)\right], \quad (3.2)$$

where r is the mixing ratio of water vapor. Potential temperature θ_L and temperature T_L at the LCL defined, respectively,

$$\theta_L = T\left(\frac{p_0}{p-e}\right)^{\frac{R_d}{C_{pd}}}\left(\frac{T}{T_L}\right)^{0.28r}, \tag{3.3}$$

$$T_L = \frac{1}{\frac{1}{T_d-56}+\frac{log_e\left(\frac{T}{T_d}\right)}{800}} + 56, \tag{3.4}$$

where T and T_d are the temperature and dew point temperature of the air at a pressure at the point p, and p_0 is reference pressure as 1000 hPa. e is the water vapor pressure, R_d and C_{pd} are the specific gas constants and specific heat capacities of dry air, respectively.

High EPT (higher than 350 K) was found on the east side of Awaji Island and above the Kii Channel (Fig. 3.9a). This indicates that warm and humid air is advected by the south-southwesterly along the western part of the Pacific high-pressure system. The south-southwesterly with high EPT along the east side of Awaji Island formed large MFC with the westerly (Fig. 3.6). In the vertical cross-section on the lines AO and BO in Fig. 3.9a (Figs. 3.9b, c), high EPT air reached the Kinki district below a height of 1 km. This indicates that the south-southwesterly brought warm and humid air to the Kinki district and caused the convergence zone with the westerly.

Figure 3.10 shows the vertical projections of the maximum values of total hydrometeor mixing ratios (cloud water, rain, ice, snow, and graupel) in a northwest-southeast direction in the dotted box in Fig. 3.5a during the formation of the SLPS from 1000 UTC to 1200 UTC. New convective cells (from Cs1 to Cs6 in Fig. 3.10) formed successively on the upwind side

of pre-existing cells, and rapidly developed over a 12 km height and traveled northeastward by the southwesterly above a height of 1 km (see Fig. 3.5). The continuous inflow of warm and humid air promoted the formation of new cells (Houze 1993; Kato and Goda 2001). The new cells were organized into the SLPS with pre-existing cells, which resulted in long-duration precipitation in almost the same area. The wind also veering from the lower to upper layers was a favorable condition for SLPSs formation (not shown, Kato 2020).

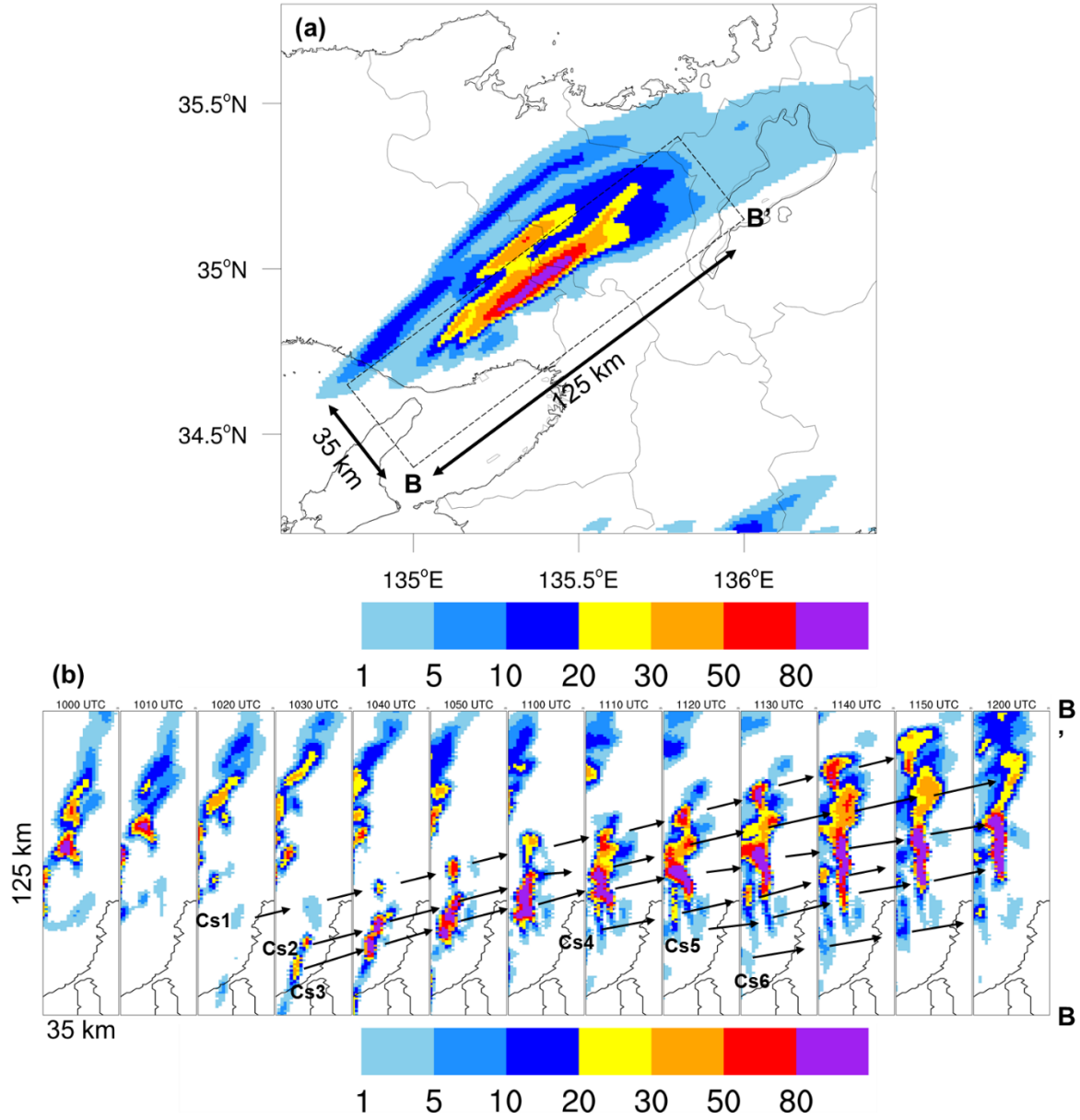

Fig. 3.5 (a) Accumulated rainfall amounts (mm) over the Kinki district from 1000 UTC to 1200 UTC 1 September 2015, depicted from the simulation results in CNTL1 (b) Rain fall rates (mm h^{-1}) in the dashed rectangle in (a) from 1000 UTC to 1200 UTC. Cs1, Cs2, Cs3, Cs4, Cs5, and Cs6 indicate simulated individual convective cells, and arrows show their movements.

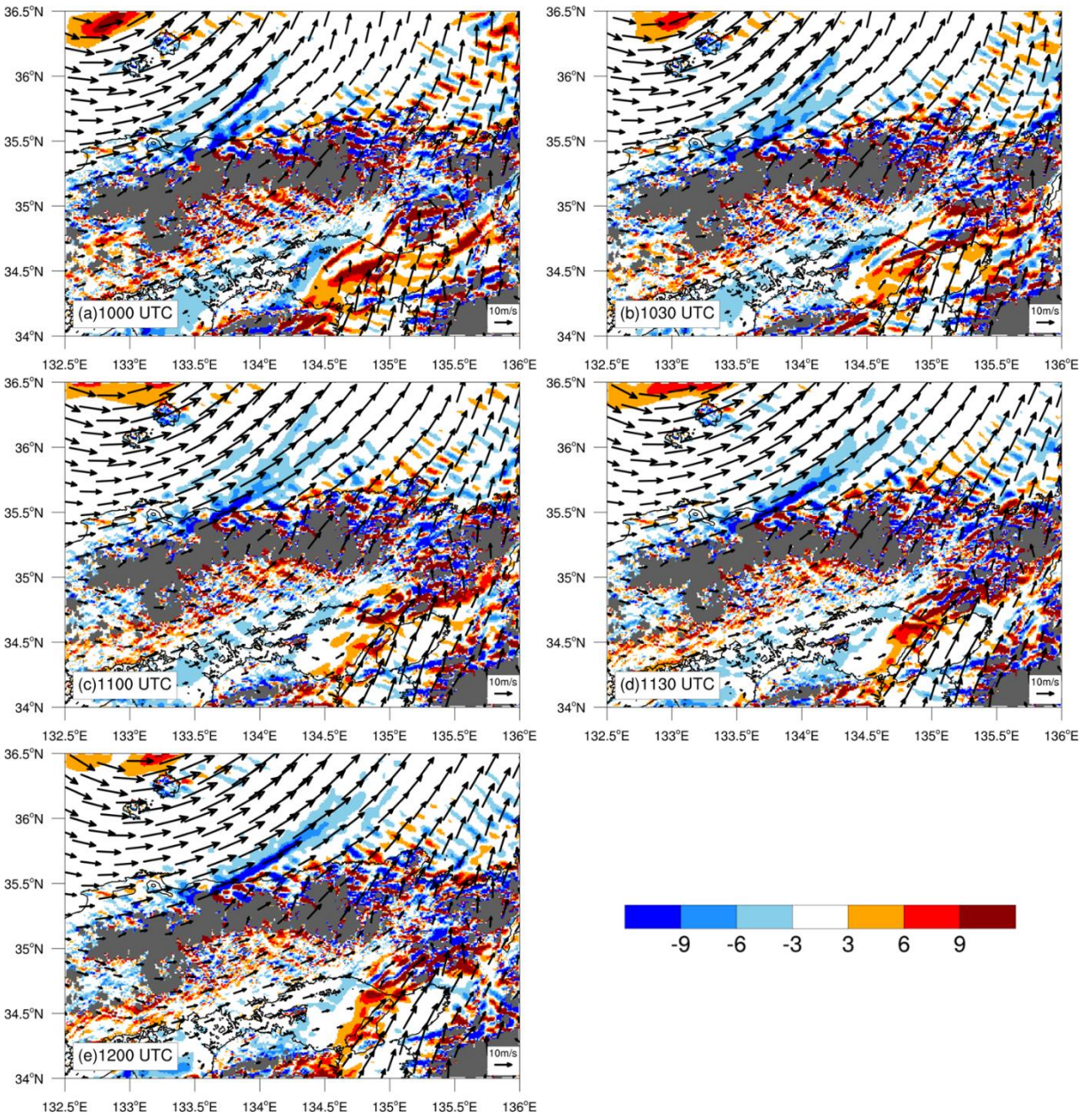

Fig. 3.6 (a-e) Moisture flux convergence (10^{-6} g kg^{-1}s^{-1}) and horizontal wind vectors at a height of 521 m from 1000 UTC to 1200 UTC 1 September 2015, depicted from the simulation results in CNTL1. Warm and cold colors indicate moisture flux convergence and divergence, respectively. Areas below a height of 521 m are masked by gray color.

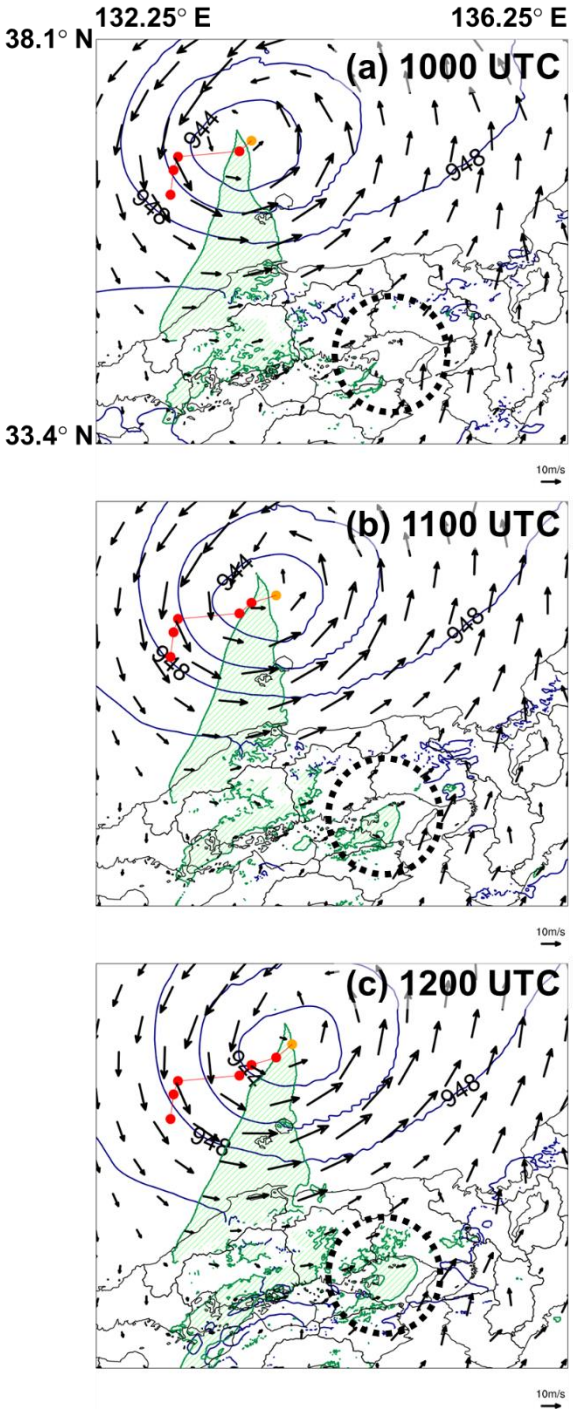

Fig. 3.7 Pressure (blue lines, hPa) and wind vectors (black arrows) at a height of 521 m in CNTL1 at (a) 1000 UTC, (b) 1100 UTC, and (c) 1200 UTC 1 September 2015. The red dots are the past centers of the extratropical cyclone every hour from 0600 UTC, and the orange

point marks the center of the extratropical cyclone at the time of each plot. The shaded region (green) denotes the westerly wind region at a height of 521 m (from 247.5° to 292.5° in azimuth).

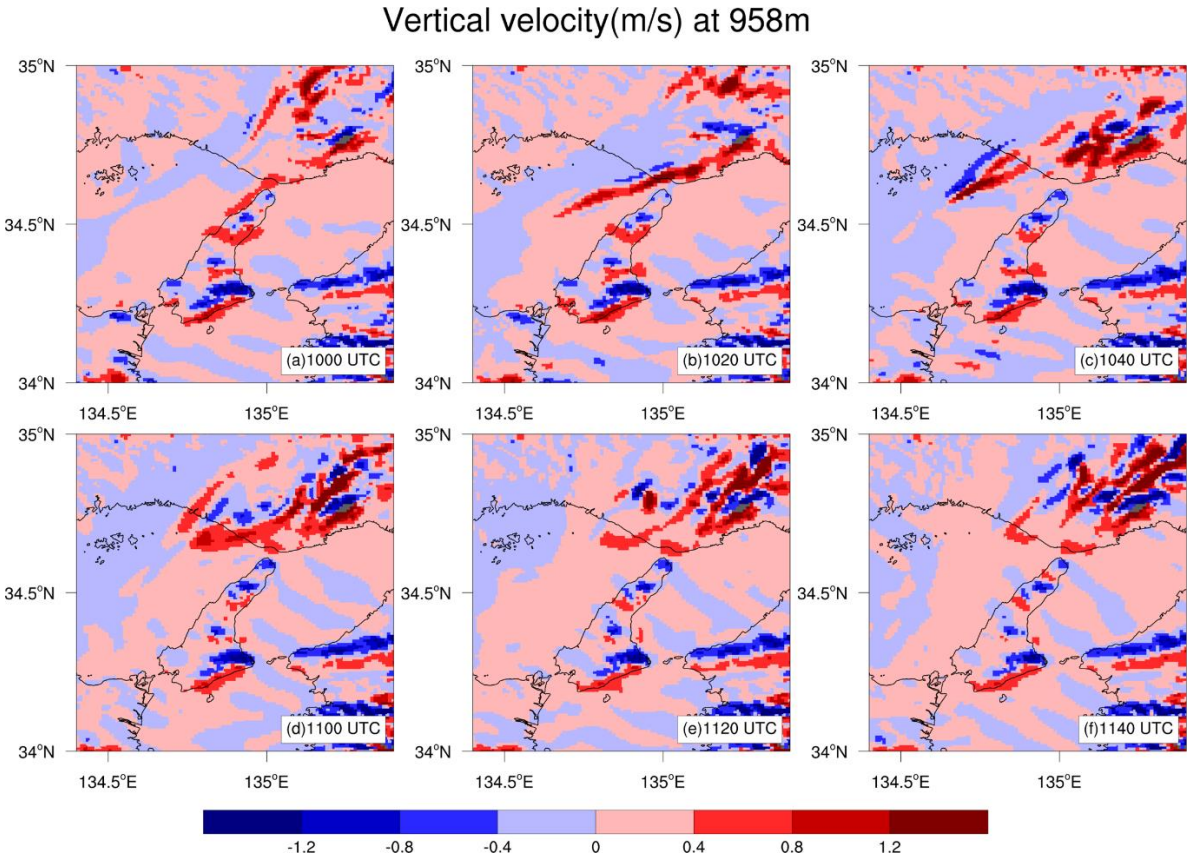

Fig. 3.8 Vertical velocities (m s^{-1}) distribution at a height of 958 m from 1000 UTC to 1140 UTC 1 September 2015. Warm and cold colors indicate updrafts and downdrafts, respectively. Areas below a height of 958 m are masked by gray color.

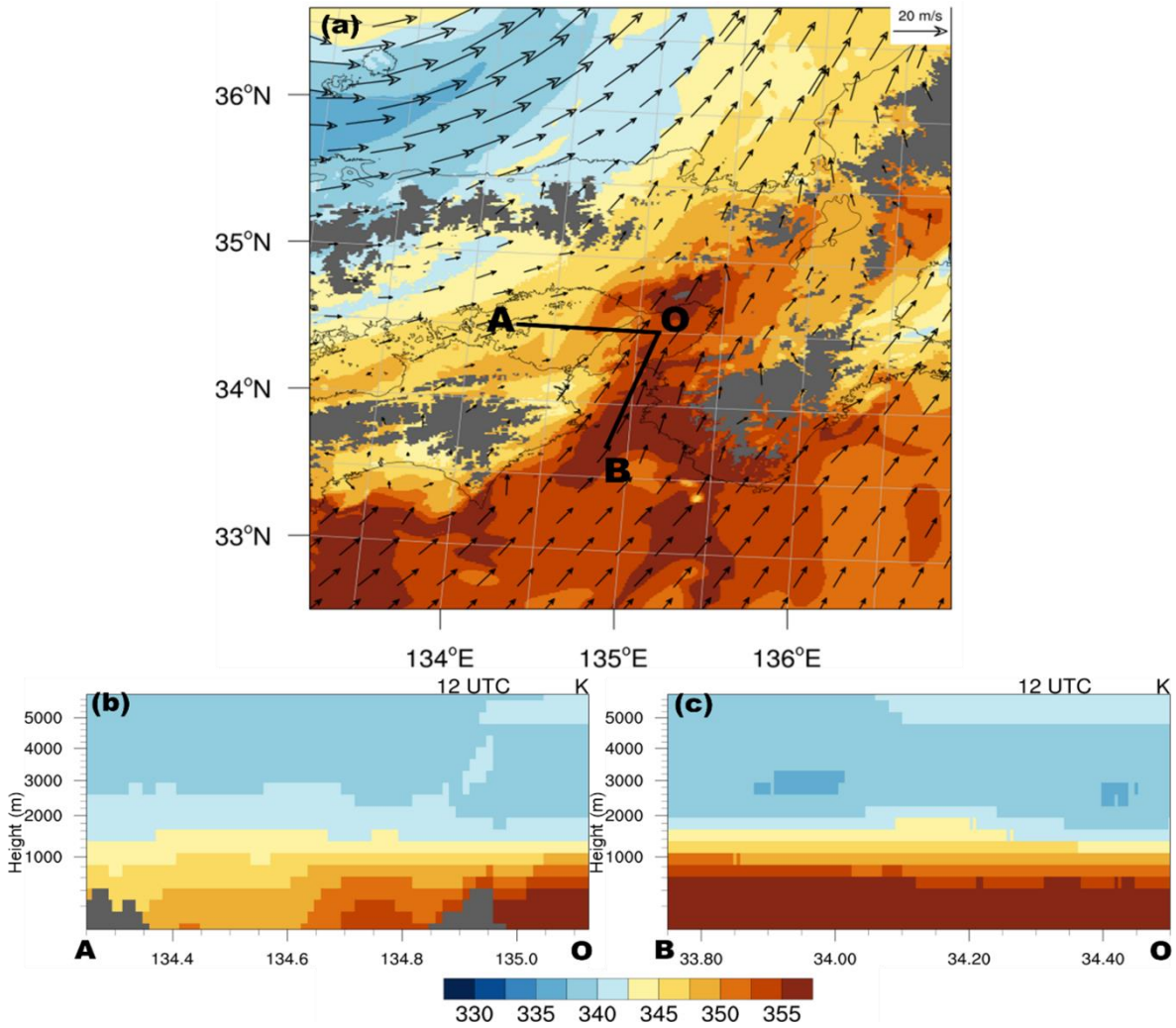

Fig. 3.9 (a) Equivalent potential temperature (EPT) distribution at a height of 521 m at 1200 UTC 1 September. Vertical cross-sections along the lines of (b) AO and (c) BO. Arrows in (a) are the horizontal winds. Areas below a height of 521 m are masked by gray color.

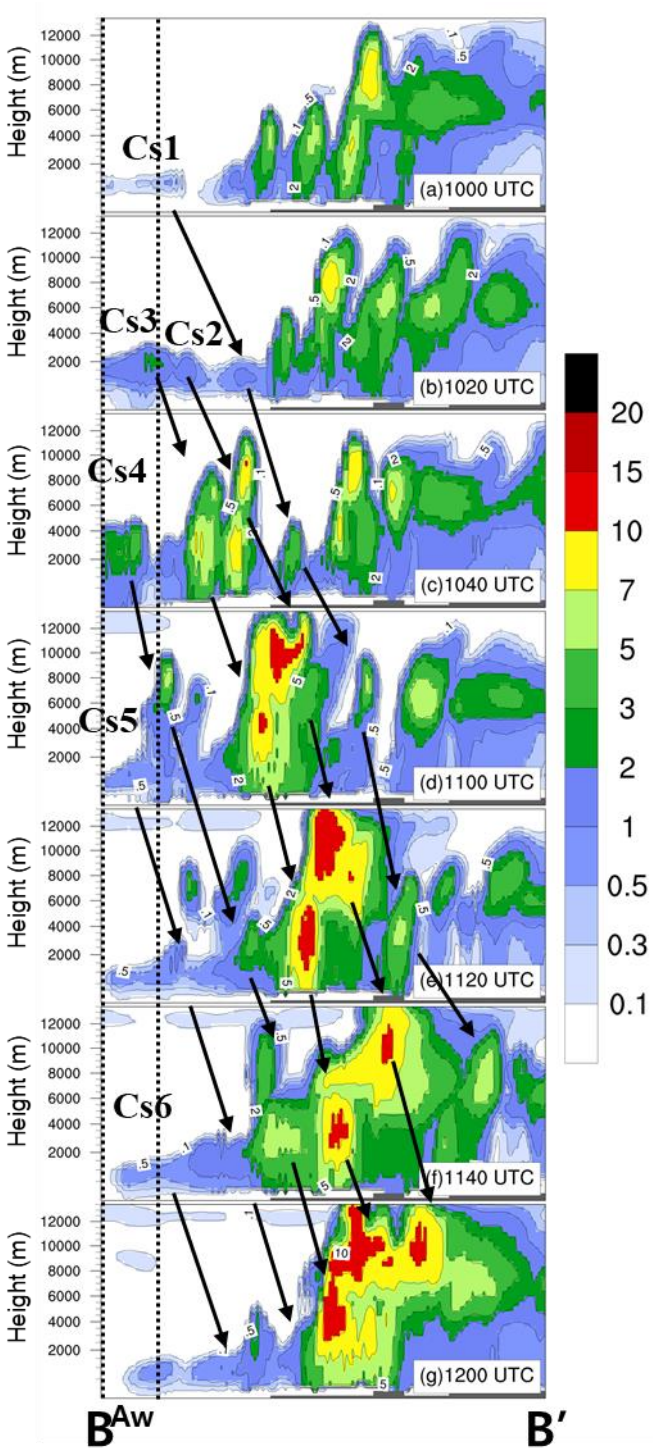

Fig. 3.10 Stretched vertical projection of the maximum hydrometeor mixing ratio (g kg^{-1}), consisting of cloud water, rainwater, snow, graupel, and cloud ice, in a northwest-southeast direction in the dashed box of Fig. 3.5a between 1020 UTC and 1200 UTC 1 September 2015.

Cs1 to Cs6 mark the same individual convective cells shown in Fig. 3.5. Area under the ground are masked by gray color. The term “Aw” and region between dotted lines denote Awaji Island.

3.2.3 Sensitivity experiments

To clarify the essential factors of the SLPS formation, sensitivity experiments were conducted with respect to environmental conditions and orography.

First, to understand the effects of environmental conditions, EXP_00 was performed with an initial condition at 0000 UTC on 1 September 2015. Figure 3.11 shows the result of EXP_00 and the difference of EPT at a height of 521 m from CNTL1 at 1200 UTC. In EXP_00, no SLPS formed over the Kinki district (Fig. 3.11a). Moreover, the convergence zone found in CNTL1 weakened, the southwesterly was dominant and the westerly was not present over the Kinki district (Fig. 3.11b). The differences in EPT at a height of 521 m between CNTL1 and EXP_00 were negative in all areas of the Kinki district; especially, there were large negative values (over 9 K) from the Kii Channel to the Osaka Plain. This indicates that the inflow to the Kinki district in EXP_00 was less warm and less humid than that in CNTL1, which did not make the atmosphere unstable over the Kinki district. Consequently, the formation of convective cells was suppressed in EXP_00.

Previous studies have shown that the formation of SLPSs in the Kinki district was caused by orography effects such as Mount Rokko or Awaji Island (Higashi et al. 2010; Ishihara and Takara 2018). To investigate the role of the topography surrounding Osaka Bay, several sensitivity experiments were conducted for the orography. Figure 3.12 shows the differences in accumulated two-hour precipitation amounts from 1000 UTC to 1200 UTC between CNTL1

and the sensitivity experiments. The area with the maximum precipitation amount in all of the sensitivity experiments shifted from that in CNTL1. The ROKKO_100M (Fig. 3.12d) showed weak precipitation amounts of 5-10 mm over Mount Rokko. In particular, the precipitation amounts on the leeward side (dashed circle) of Mount Rokko was higher than those in CNTL1. In AWAJI_NONE and AWAJI_0M (Figs. 3.12b, c), the SLPS shifted slightly to the west; however, the shape of the SLPS was similar to that in CNTL1. In contrast, in SHIKOKU_NONE and SHIKOKU_0M (Figs. 3.12e, f), the SLPS shifted to the southeast relative to CNTL1, and the total precipitation amounts became larger.

The MFC and horizontal wind vectors at a height of 521 m in the sensitivity experiments at 1000 UTC 1 September 2015 are compared with those in CNTL1 (Fig. 3.13). The shape and intensity of convergence zones along the west of Awaji Island in AWAJI_NONE, AWAJI_0M and ROKKO_100M (Figs. 3.13b, c, and d, respectively) were similar to those in CNTL1 (Fig. 3.13a). In AWAJI_NONE (Fig. 3.13b), the MFC in the convergence zone became slightly smoother, and the linear shape was clearer in comparison with CNTL1. In AWAJI_0M (Fig. 3.13c), the MFC became weaker in the north of Awaji Island and over Awaji Island. In SHIKOKU_NONE and SHIKOKU_0M (Figs. 3.13e, f), a large convergence area found on the northwest side of Awaji Island in the other experiments shifted to the southwest of Awaji Island, and the horizontal velocity field was also different in the Kinki district. These results indicate

that Shikoku Island altered the low-level wind field to determine the location of the SLPS formation.

Table 3.2 summarizes the results in CNTL1 and the sensitivity experiments. The EPT and MFC values were averaged within the dashed square in Fig. 3.13a at a height of 521 m. All of the experiments except EXP_00 reproduced the SLPS, in which the EPT at a height of 521 m (EPT521m) exceeded 352K. In EXP_00, the MFC at a height of 521 m (MFC521m) was significantly smaller than the other experiment, which was one of the reasons why the SLPS was not reproduced.

In SHIKOKU_NONE and SHIKOKU_0M (Figs. 3.13e, f), the MFC521m became higher than that in CNTL1. It indicates that if Shikoku Island was removed, more water vapor would flow into the Osaka Bay, which could result in large precipitation amounts. Consequently, the large precipitation would be generated by the strong convergence than that in CNTL1. The MFC in ROKKO_100M was similar to that in CNTL1, while in AWAJI_0M and AWAJI_NONE, the MFC was slightly weaker over Awaji Island. These results indicate that Awaji Island slightly affected the intensity of the convergence zone; however, it did not largely change the precipitation amounts (Fig. 3.12).

These sensitivity experiments indicate that the topography surrounding Osaka Bay, particularly Mount Rokko (931 m height) and Awaji Island (608 m height), can modify the low-level convergence, as well as the topography in Shikoku Islands. In particular, the location

of the convergence zone shifted depending on the roughness of Awaji Island. AWAJI_0M and AWAJI_NONE showed that the difference in roughness due to land-use changes the MFC, as presented by Tsuguti and Kato (2014a).

As mentioned above, the topography surrounding Osaka Bay slightly altered the location and precipitation amounts of the SLPS, although it was not the essential formation factor of the SLPS over the Kinki district on 1 September 2015. Nevertheless, Shikoku Island altered the winds in the lower layer and the convergence zone caused by the westerly and south-southwesterly.

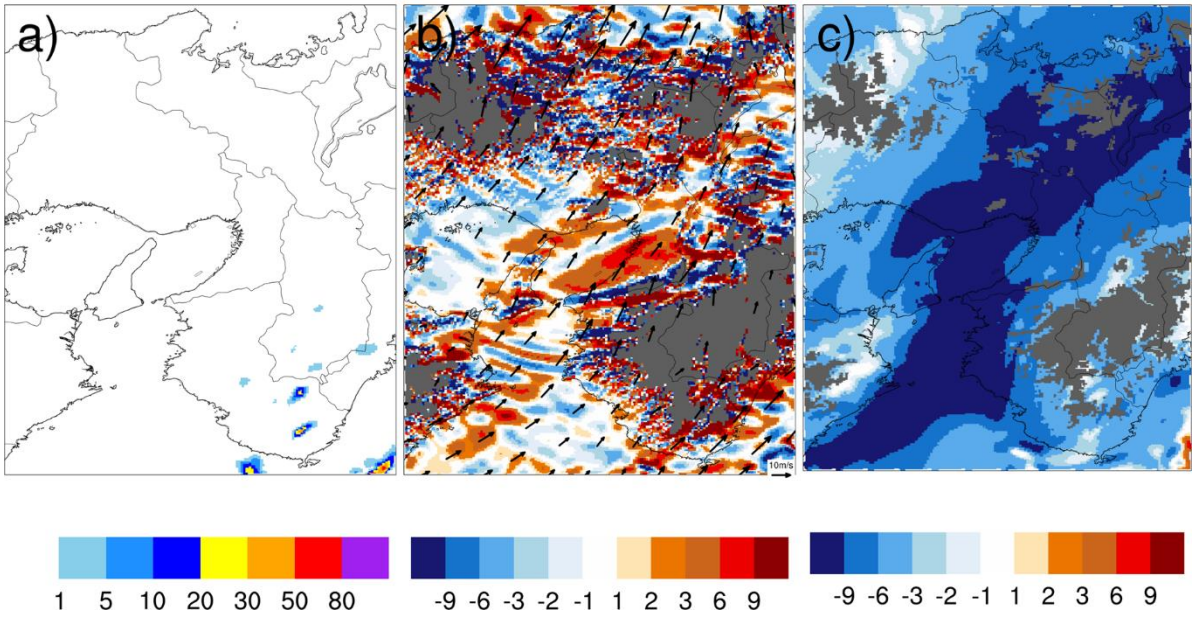

Fig. 3.11 (a) Precipitation intensity (mm h^{-1}), and (b) moisture flux convergence (MFC, 10^{-6} g $kg^{-1}s^{-1}$) and horizontal wind at a height of 521 m in EXP_00 at 1200 UTC 1 September 2015. Areas below a height of 521 m are masked by gray color. (c) Same as (b), but the differences of EPT (K) between EXP_00 and CNTL1.

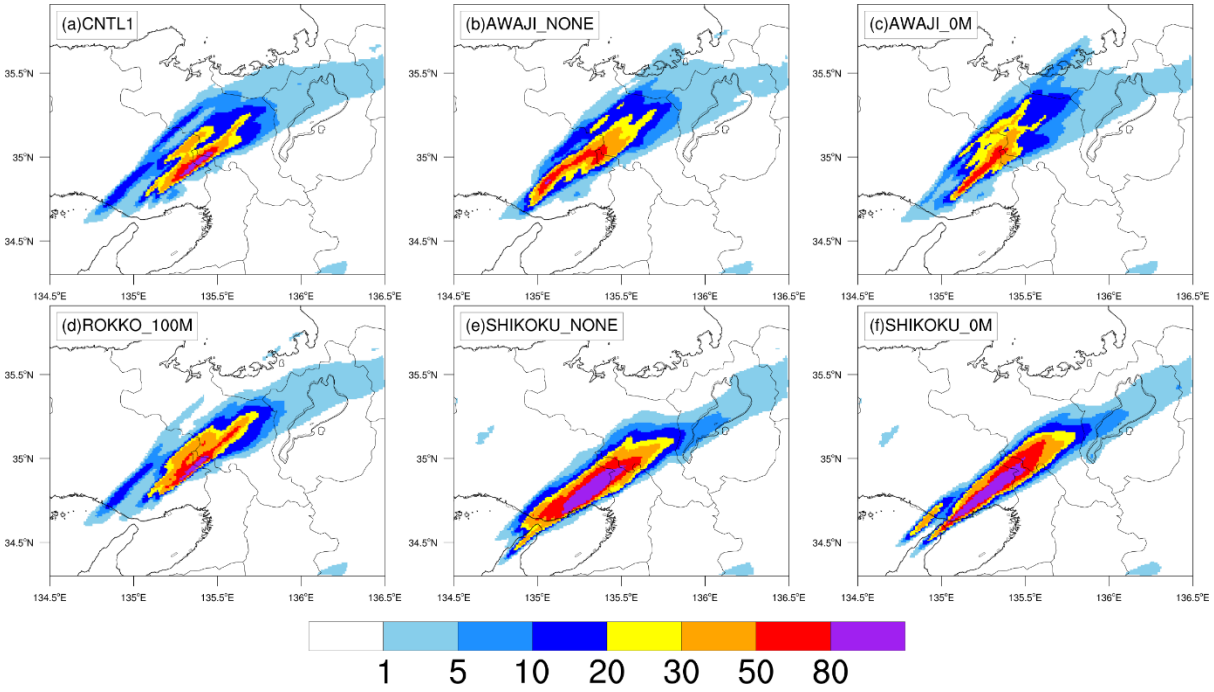

Fig. 3.12 Accumulated two-hour precipitation amounts in (a) CNTL1, (b) AWAJI_NONE, (c) AWAJI_0M, (d) ROKKO_100M, (e) SHIKOKU_NONE, and (f) SHIKOKU_0M from 1000 UTC to 1200 UTC 1 September 2015.

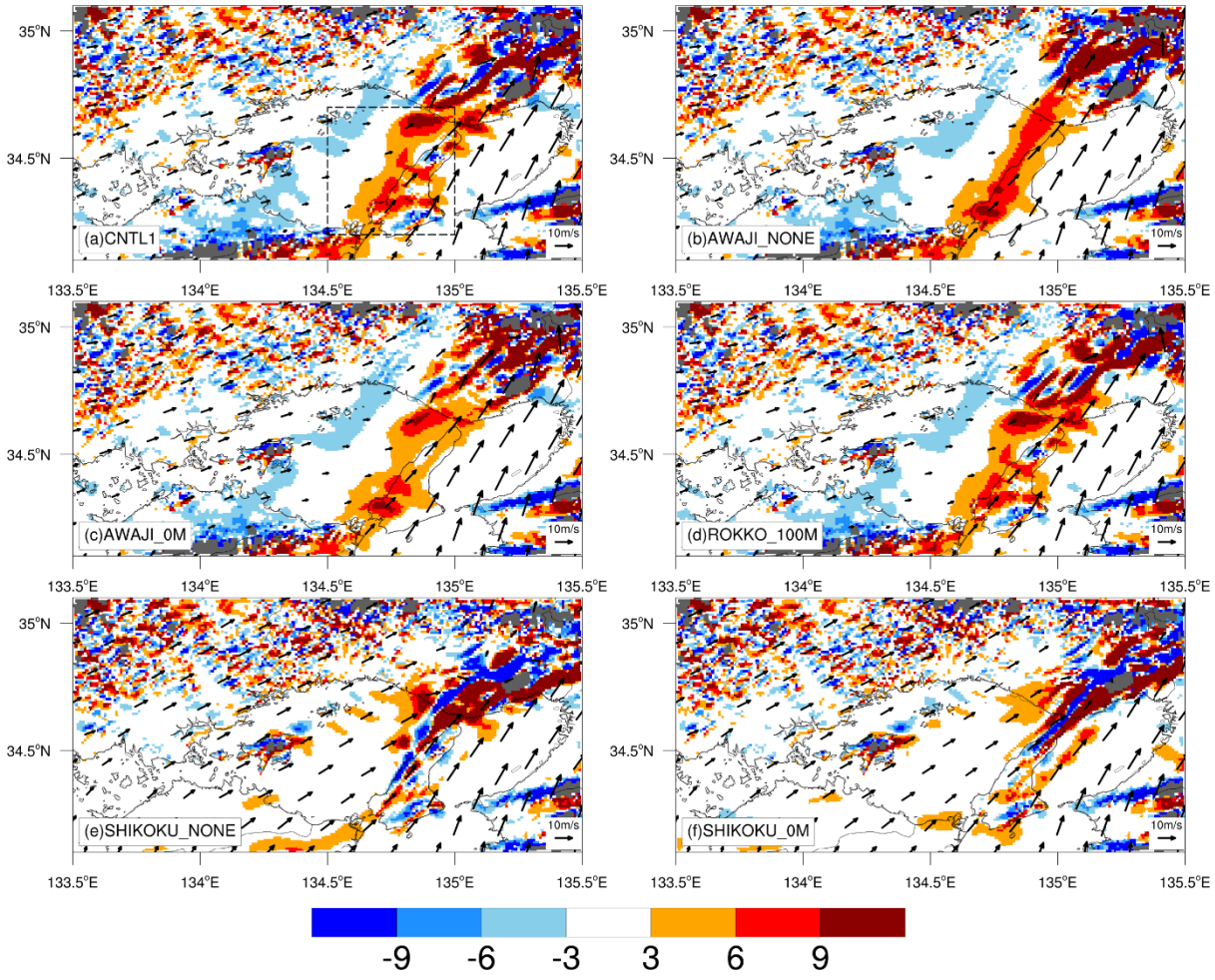

Fig. 3.13 Moisture flux convergence (MFC, 10^{-6} g kg^{-1}s^{-1}) and horizontal wind vectors in (a) CNTL1, (b) AWAJI_NONE, (c) AWAJI_0M, (d) ROKKO_100M, (e) SHIKOKU_NONE, and (f) SHIKOKU_0M at a height of 521 m at 1000 UTC 1 September 2015. The dashed rectangle in (a) is the averaged region for EPT and MFC shown in Table 3.2.

Table 3.2 SLPS reproduction, moisture flux convergence (MFC) and equivalent potential temperature (EPT) averaged within the dashed square in Fig. 3.13a at a height of 521 m for CNTL1 and sensitivity experiments (EXP_00, ROKKO_100M, AWAJI_NONE, AWAJI_0M, SHIKOKU_NONE, and SHIKOKU_0M) at 1200 UTC 1 September 2015.

Experiment (12 UTC)	**SLPS reproduction**	**Average MFC** ($10^{-6} \times \mathrm{g\,kg^{-1}s^{-1}}$)	**Average EPT (K)**
CNTL1	Yes	3.48	353.9
EXP_00	No	0.75	341.3
ROKKO_100M	Yes	3.64	353.7
AWAJI_NONE	Yes	3.20	353.9
AWAJI_0M	Yes	3.10	354.0
SHIKOKU_NONE	Yes	5.77	352.9
SHIKOKU_0M	Yes	4.95	353.1

3.3 Discussion

On the basis of CNTL1 and the sensitivity experiments, the formation mechanisms of the SLPS were investigated that occurred on 1 September 2015 in the Kinki district. For the SLPS formation mechanisms, previous studies often considered the following two essential factors for the development of convective cells; the orographic effect and large-scale forcing. This event could be caused by different formation factors from those two factors.

First, the orographic effect, which lifts low-level air (Ishihara and Takara 2018) or forms a low-level convergence zone (Kurihara et al. 2009; Takasaki et al. 2019), has been considered to be one of the essential factors in the formation of SLPSs. As shown in Fig. 1.4, the average heights of Mount Rokko and Awaji Island were lower than the LFC (958 m in height) of the air parcel lifted from a height of 521 m. This LFC was higher than that in the SLPS event studied by Ishihara and Takara (2018) (approximately 470 m in height). Moreover, Awaji Island did not trigger for the SLPS formation in this event. According to these results, the topography surrounding Osaka Bay was not an essential factor for the SLPS formation in this event. However, SHIKOKU_NONE and SHKOKU_0M altered the pattern of low-level winds, i.e., the shape and location of the convergence zone. These results indicate that Shikoku Island blocks the low-level southwesterly.

Second, other previous studies have suggested that a large-scale forcing, such as a cold front, was an essential factor for generating a convergence zone (Kato and Goda 2001; Kato 2006;

Seko et al. 2006; Higashi et al. 2010; MRI 2010; Kato 2020). However, no large-scale forcings were found in the observation data and numerical experiments in this study. Figure 3.14 shows the EPT and horizontal wind vectors at a height of 958 m in CNTL1 at 1030 UTC and 1130 UTC. The horizontal shear zone between the extratropical cyclone with relatively low EPT and the Pacific high-pressure system with high EPT was stagnant to the north of the Kinki district (Fig. 3.14a, dotted circle). It indicates that the large-scale shear was not essential for the SLPS formation mechanism in this case.

In this event, the low-level convergence between the westerly and south-southwesterly played the role of the weak forcing that led to the generation of convective cells, as in the case studied by MRI (2010). To understand the essential factors of the SLPS formation in this event, the characteristics of the south-southwesterly and westerly at low levels were further investigated.

The Pacific high-pressure system located to the south of the Kinki district caused the warm and humid inflow to the Kinki district through the Kii Channel, which made the atmosphere conditionally unstable in the Kinki district. The water vapor mixing ratio in Osaka Bay below a 203 m height (34.5° N 135.2° E) was larger than 20 g kg^{-1} (not shown). Under such a highly humid condition in the lower layer, weak forcing can trigger convective cells. The weak forcing maintained an average of 0.2 m s^{-1} in vertical velocity at a height of 958 m within the dashed square in Fig. 3.13a over the convergence zone from 1000 UTC to 1200 UTC.

To investigate the relationship between the westerly region associated with the extratropical cyclone and the warm and humid south-southwesterly in the Kinki district, the pressure and winds at a height of 521 m were compared in CNTL1 between 1000 UTC and 1200 UTC on 1 September 2015 (Fig. 3.7) with those in EXP_00 (Fig. 3.15). In EXP_00, the northeast movement of the extratropical cyclone center (blue and orange points) was slower than that in CNTL1 (red marks). In addition, the eastward extension of the westerly region associated with the extratropical cyclone was delayed in comparison with that in CNTL1 (Figs. 3.15a, b, and c dotted circle). After four hours later (1600 UTC), a convergence zone also formed on the east coast of Awaji Island in EXP_00 when the westerly region reached Awaji Island, but the EPT521m in the south-southwesterly inflow was lower than that in CNTL1 (around 345 K, not shown). Consequently, the atmosphere was conditionally stable, the SLPS did not form even at that time (not shown). This result indicates that not only large MFC but also high EPT521m was important for the SLPS formation.

To evaluate the environmental conditions for the SLPS formation, six favorable occurrence conditions were used proposed by Kato (2020) and examined them in all of the numerical experiments (Table 3.3). Parameters for the six conditions are the water vapor flux amount at a 521 m height (FLWV), dLFC, RH at 500 and 700 hPa (RH500 and RH700), SREH, synoptic-scale upward velocity (400km mean field at 700 hPa, W700), and equilibrium level estimated from 521 m height data (EL). Detailed descriptions of the six conditions are given in Kato

(2020). This study used a 521 m vertical layer of numerical experiments, instead of a height of 500 m used in Kato (2020). The average values of these conditions were evaluated within the square of 50 km × 50 km in Fig. 3.13a.

All of the conditions were satisfied for the SLPS formation at 1200 UTC on 1 September 2015 in the numerical experiments, except for EXP_00. On the other hand, the SLPS could not be reproduced in EXP_00 because the conditions related to FLWV, dLFC, RH500, RH700, and EL were not satisfied. This ascertains that the water vapor at low and middle levels were more important than other factors in the present case.

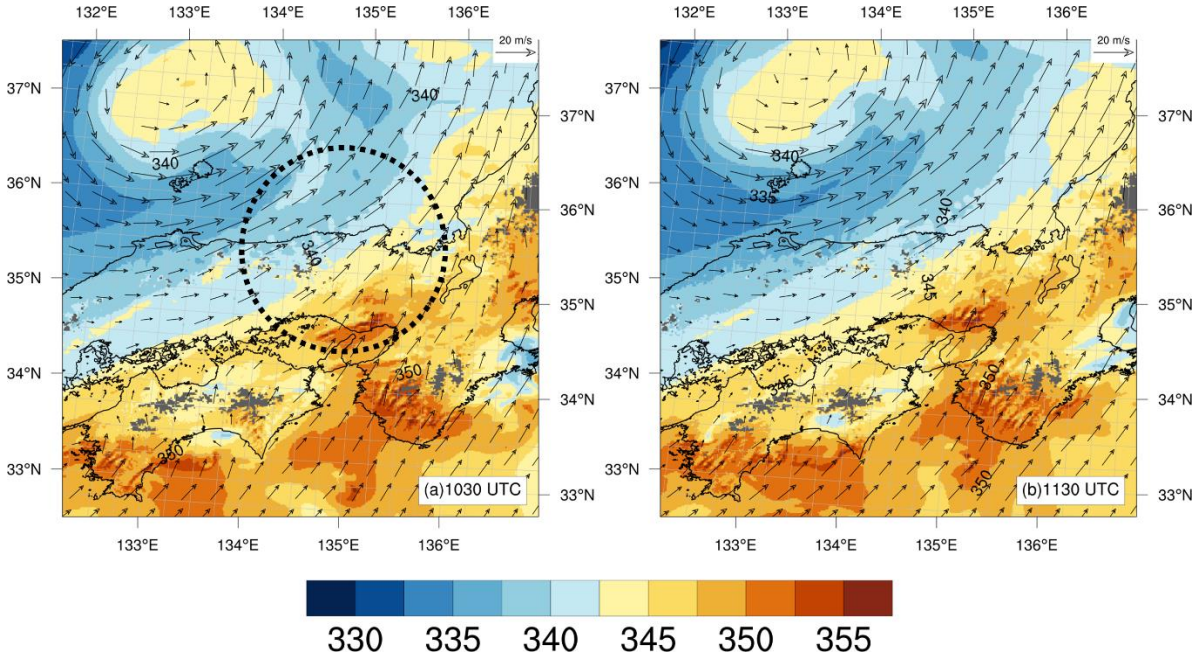

Fig. 3.14 Distributions of EPT (K) at a height of 958 m in CNTL1 at (a) 1030 UTC and (b) 1130 UTC 1 September 2015.

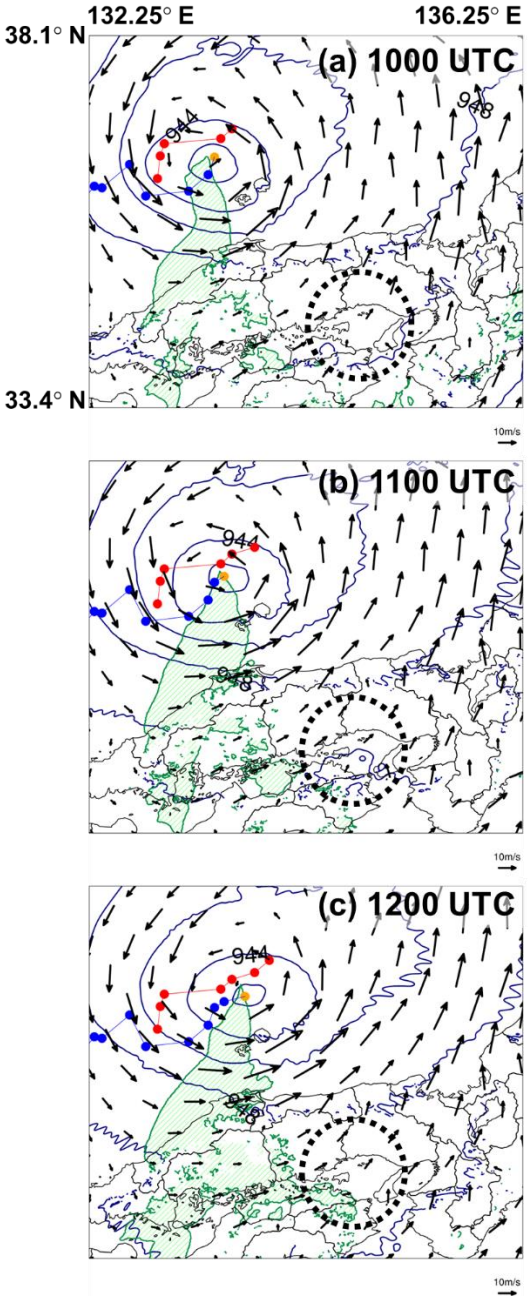

Fig. 3.15 Same as Fig. 3.7, but in EXP_00. The blue dots mark the past centers of the extratropical cyclone, and the orange point marks the center of the extratropical cyclone at the time of each plot. The red dots indicate the path of the extratropical cyclone center in CNTL1 shown in Fig. 3.7.

Table 3.3 Six favorable occurrence conditions of SLPSs in CNTL1 and sensitivity experiments (EXP_00, ROKKO_100M, AWAJI_NONE, AWAJI_0M, SHIKOKU_NONE, and SHIKOKU_0M) at 1200 UTC 1 September 2015. FLWV denotes the water vapor flux amount at a 521 m height, dLFC denotes the distance to the level of free convection from 521 m for lifted air, RH500 and RH700 respectively denote the relative humidity at 500 and 700 hPa, SREH denotes the storm relative environmental helicity, W700 denotes the synoptic-scale upward velocity (400km mean field at 700 hPa), and EL denotes the equilibrium level estimated from a 521 m height. Detailed descriptions of the six conditions are given in Kato (2020). The average values of these conditions were evaluated within the square of 50 km × 50 km in Fig. 3.13a (34.418° N, 134.7° E).

Experiment (12 UTC)	**FLWV ($\mathbf{g\,m^{-2}s^{-1}}$)**	**dLFC (m)**	**RH500 (%)**	**RH700(%)**	**SREH ($\mathbf{m^2s^{-2}}$)**	**W700 ($\mathbf{m\,s^{-1}}$)**	**EL (m)**
CNTL1	152.4	437	74.7	81.7	113.67	0.017	12102
EXP_00	113.2	-	39.7	72.3	122.45	0.018	-
ROKKO_100M	152.6	437	74.6	81.5	113.66	0.017	12102
AWAJI_0M	152.1	437	75.1	81.4	114.11	0.016	12102
AWAJI_NONE	149.3	437	76.1	82.1	111.08	0.016	12102
SHIKOKU_0M	175.2	95	72.7	83.6	110.52	0.012	12102
SHIKOKU_NONE	183.6	95	73.9	84.9	99.24	0.015	12541
Kato (2020)	> 150	< 1000	> 60	> 60	> 100	> 0	> 3000

4. Case2: SLPS over Tokai district highlands on 7 July 2018

4.1 The environmental conditions over Tokai district on 7 July 2018

In July 2018, a heavy rainfall event occurred in western and central Japan (Fig. 1.4), which is named Heavy Rainfall Event Japan in 2018 (HREJ2018) by the Japan Meteorological Agency (JMA). According to JMA (2018), the heavy rainfall of this event was observed in the wide area of western Japan and Gifu prefecture in Tokai district. In this event, 15 precipitation systems of SLPS were identified using the detection technique of JMA (2018). Among them, the SLPS of the second-highest total precipitation amount (1214. 5 mm) was observed in Gifu prefecture. The total precipitation amounts at the Hirugano AMeDAS (36.01° N, 136.893° E, Fig. 1.4) point from 6 to 7 July 2018 is 623 mm, which is almost a half of the total precipitation amount at this point during HREJ2018. Two heavy rainfall (HR) periods over 80 mm of three-hour rainfall intensity were present; HR1 (from 0700 UTC to 1100 UTC 6 July 2018) and HR2 (from 2300 UTC 6 July to 0300 UTC 7 July 2018). Total precipitation amounts in HR1 and HR2 are 179 and 131.5 mm, respectively. In this study, the HR2 period was studied because the SLPS was clearly observed in this period. However, this SLPS was not included in the 15 of SLPS in the previous study (JMA, 2018). There was no sudden change in the temperature and wind during the HR2 at the Nagataki AMeDAS (35.953° N, 136.832° E, Fig. 1.4) (not shown). This indicates that no large system passed over Tokai district during SLPS formation.

The JMA radar showed characteristics of the SLPS during the HR2. Figure 4.1 shows the distribution of the total precipitation amount and time evolution of the SLPS during the HR2. The large total precipitation amount of the SLPS extended from the southwest to the northeast just above the Hirugano AMeDAS (Asterisk mark in Fig4.1a). The maximum total precipitation amount of the SLPS was 141.9 mm during the HR2 period. When the SLPS began to form, scattered convective cells formed around the highlands (green oval in Fig. 4.1b). Then, the convective cells CC1 and CC2 appeared on the windward side at 2330 UTC and traveled northward and northeastward with developing (Fig. 4.1b). New convective cells CC3 and CC4 began to develop at 0010 and 0020 UTC, respectively. They showed the similar behavior to CC3 and CC4. The successive developments of convective cells resulted in the formation of the SLPS around 0030 UTC. In addition, another convective cell group (a convective line) was generated on the southeast side of the SLPS (red solid oval in Fig. 4.1b) and they merged to the SLPS with time. At 0150 and 0210 UTC, CC5 and CC6 began to develop, respectively. Other convective lines also formed at 0220 and 0250 UTC (red dotted ovals in Fig. 4.1b) and merged with the SLPS. Consequently, the total precipitation amount of the SLPS was enhanced. The formation process of the SLPS seems to have characteristic of both the back-building and back-and-side-building formation processes.

Figure 4.2 shows the JMA surface weather chart at 0000 UTC 7 July 2018. The Baiu front extended from China to the Pacific Ocean through the Japanese Islands with a low-pressure

system over the Sea of Japan. The southerly and southwesterly toward the Baiu front from the Pacific Ocean were present to the south of Japan. The low-level southwesterly from the East China Sea and the southerly from the North Pacific high made a convergence and confluence to the south of Tokai district. JMA (2018) suggested that the inflow of humid air at low-levels was an essential factor of the heavy rainfall events during HREJ 2018

Figure 4.3 shows the skew T-log P upper-air diagram of the Shionomisaki station at 0000 UTC 7 July 2018. The layer below 710 hPa (3021 m height) was very humid (RH over 84 %). The wind changed from the southerly to the southwesterly with height below 1 km in height. The LCL and LFC of an air parcel averaged from the surface to 500-m height being lifted adiabatically were low levels as 962.4 hPa (approximately 433.6 m in height) and 953.6 hPa (approximately 514.7 m in height), respectively. The CAPE and CIN estimated by lifting a parcel from a 500-m height were 724.5 J kg^{-1} and 0.0 J kg^{-1}, respectively. The TPW was 55.2 mm. Under the conditions with the low LCL and LFC, and zero CIN, convective cells can easily form by weak forcing at low levels.

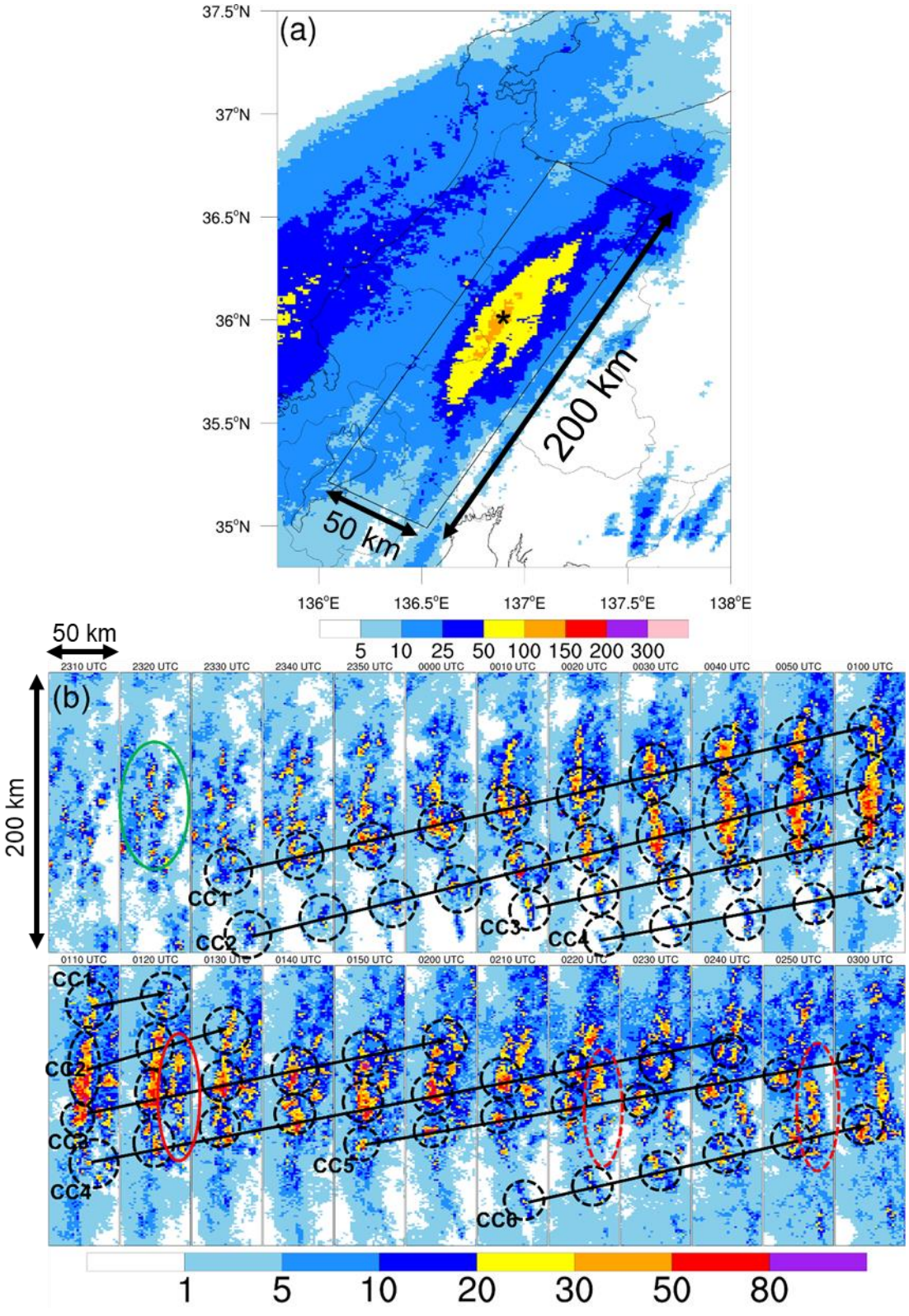

Fig. 4.1 (a) Total precipitation amounts (mm) over Tokai district from 2300 UTC 6 July to 0300 UTC 7 July 2018, obtained from the JMA radar. The rectangle indicates the region shown

in Fig. 4.1b. (b) CAPPI displays of precipitation intensity (mm h^{-1}) at a height of 2 km from 2310 UTC 6 to 0000 UTC 7 July every 10 minutes. CC1, CC2, CC3, CC4, CC5, and CC6 denote individual convective cells, and arrows show their movements.

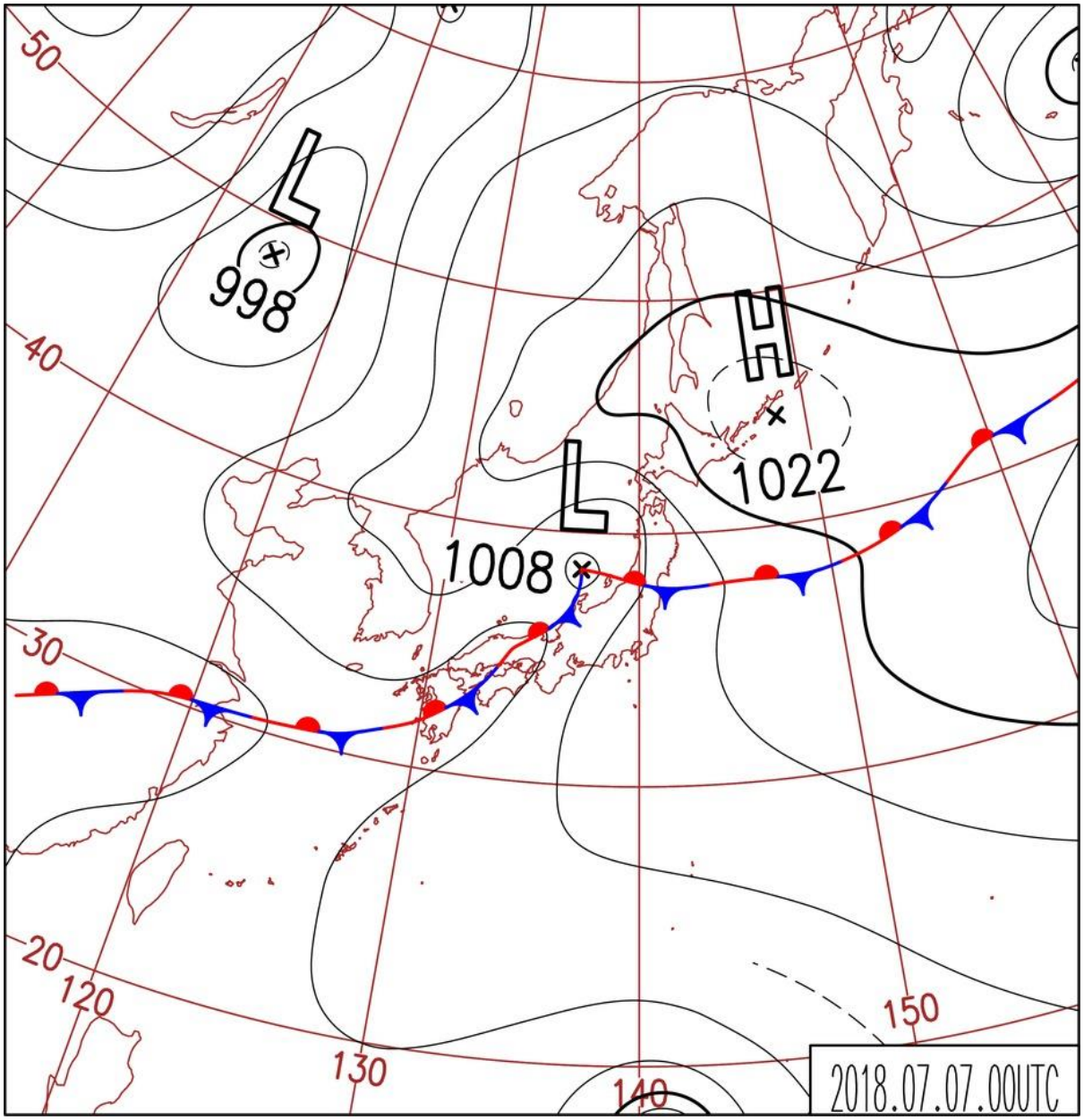

Fig. 4.2 JMA surface weather chart at 0000 UTC 7 July 2018.

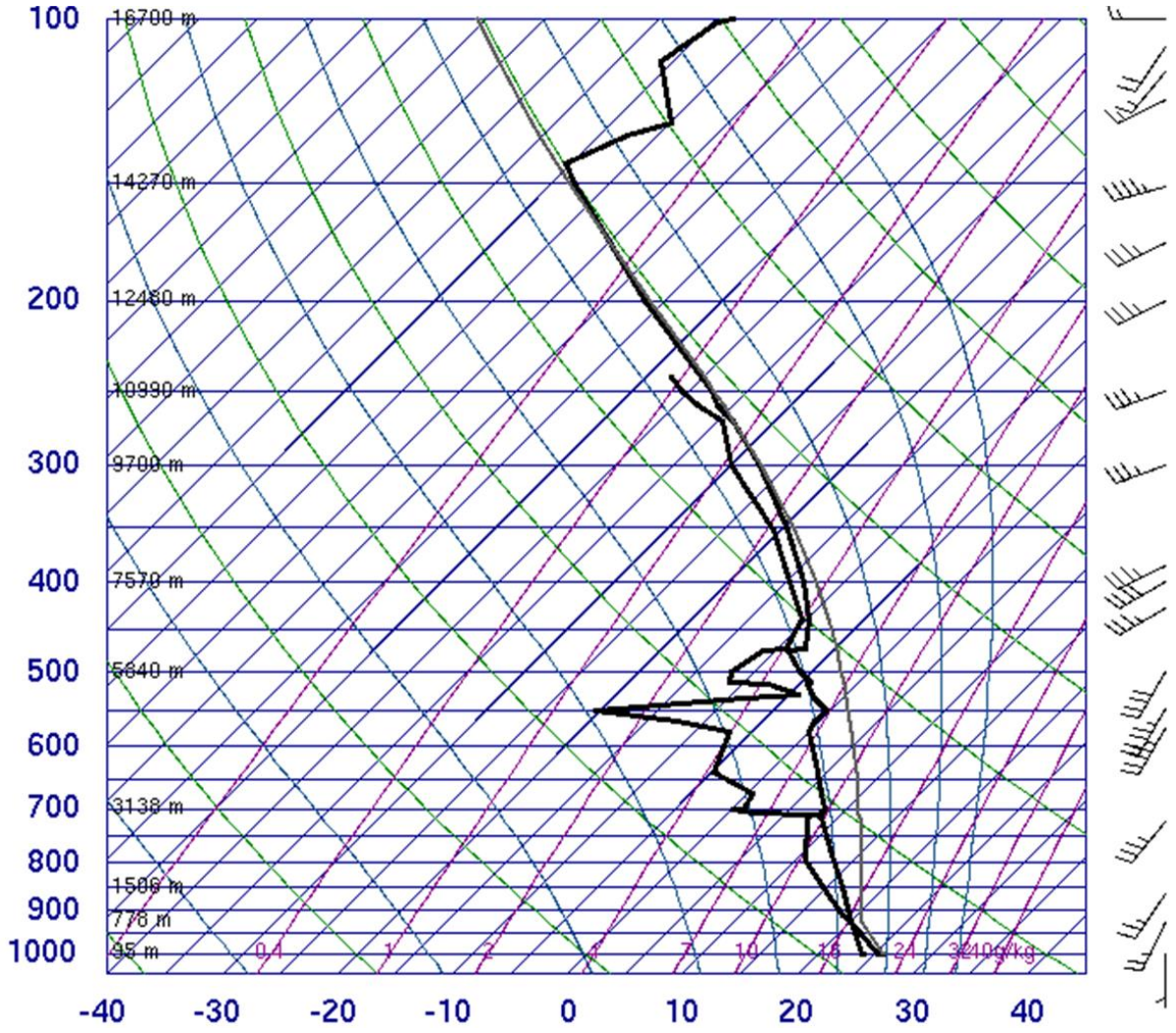

Fig. 4.3 Profiles of temperature and dew point temperature (°C) on skew T-log P diagram observed at the Shionomisaki station at 0000 UTC 7 July 2018. The full and half burbs are wind speeds of 10 knots and 5 knots, respectively.

4.2 Result

4.2.1 Numerical experiment configuration

Aims to Case2, the simulation experiment (CNTL2) and sensitivity experiments were conducted for the orography. The horizontal grid spacing is 1 km, and 70 stretched layers with the model top of 17.3 km are set in a vertical direction. Seven layers are included below 1 km. The numerical experiments were conducted for the period from 1500 UTC 6 to 0300 UTC 7 July 2018 (Table 4.1). Other numerical experiment configurations are the same as CNTL1. In sensitivity experiments for the effects of orography of Tokai district, the terrain elevation was changed. In the experiment of HT_LCL, the terrain higher than the LCL in the SLPS area (the rectangle in Fig. 1.4c) was reduced to the height of the LCL. In the experiment of HT_100M, the terrain heights in the vicinity of SLPS were set to be 100 m in the rectangle of Fig. 1.4c. The sensitivity experiments on the orography were performed with the same experimental settings as those of CNTL2.

Table 4.1 The configuration of the simulation (CNTL2) and sensitivity experiments.

Cloud Resolving Storm Simulator Ver. 3.4.3

Horizontal grid spacing	1 km (1197 x 1197)
Vertical grid spacing (Top / Bottom height)	250 m (vertically stretched grid, 70 layers) (17269 m / 25 m)
Time step	0.5 s
Initial data Boundary data	JMA-MA data (3 Hourly, 5 km)
Land-use data	USGS 30-s data
Projection	Lambert Conformal (center at 140° E, secant at 30° and 60° N)
Sub-grid parameterization	1.5-order closure with TKE prediction
Surface processes	Energy and momentum fluxes shortwave and longwave radiation
Surface model layer	33 layers (land: 0.1 m and sea: 0.3 m)
Integration period	1500 UTC 6 – 0300 UTC 7 July 2018

4.2.2 Simulation experiment

To verify the result of the CNTL2, this study compared the simulated distribution of total precipitation amount with the JMA radar observation. Figure 4.4 the total precipitation amount and time evolution of the SLPS in the CNTL2 from 2300 UTC 6 July to 0300 UTC 7 July 2018. Compared with the JMA radar observation (Fig. 4.1), the maximum of the total precipitation amount (277.7 mm) of SLPS is overestimated to that of observation (Fig. 4.4a) because the simulated SLPS began to develop earlier than the observed one and the intense period was longer than the observation. The SLPS location well agrees with that observed by the JMA radar and the distribution pattern of the total precipitation amount was also similar to that of the JMA radar observation. The time evolution of SLPS in the CNTL2 showed the successive development of convective cells which are as intense as those in observation. Similar to the observation, scattered convective cells were present in the highlands just before the beginning of HR2. The behavior of convective cells in the simulated SLPS is similar to that of the observation; scattered convective cells developed around the highlands (green oval in Fig. 4.4b), formations of convective cells (CS1, CS2, CS3, CS4, CS5, and CS6) on the windward side of the SLPS, and the secondary convective line formation to the southeast of the SLPS (red ovals in Fig. 4.4b). Although there are some discrepancies between CNTL2 and the radar observations, the location and the line-shaped pattern of the SLPS were well simulated; particularly the orientation of the SLPS and the behavior of convective cells

traveling from the southwest to the northeast. Therefore, the result of the CNTL2 were useful to study the SLPS. The simulated convective cells of and secondary convective lines were generated on the slope of highlands. Figure 4.5 shows simulated precipitation rainfall intensity with topography at 0130 UTC 7 July 2018 and MFC at a height of 600 m wind vectors averaged from 0100 UTC to 0200 UTC 7 July 2018. New convective cells of CS4, CS5 (black circles), and secondary convective line (red circle) generated on highlands slope, respectively (Fig. 4.5a). In addition, the location of these cells and moisture convergence zone at low-level were similar (Fig. 4.5b). This indicated that the slope of highlands (windward side of highlands) convergence the humid air at the low-level.

Figure 4.6 horizontal map at a height of 600 m and vertical cross-section of EPT and wind vectors averaged from 2300 UTC 6 July to 0000 UTC 7 July 2018. At a height of 600 m, the Baiu front was located over the Sea of Japan from 36 ° N to 37 ° N (Fig. 4.6a) with the southwesterly on the south side and the northeasterly on the north side. In Gifu prefecture, high EPT (higher than 350 K) was advected by the southwesterly or the southerly from the Pacific Ocean to the highlands of Gifu prefecture (from 136.6 ° E to 137 ° E). Figure 4.6a indicates that the warm and humid southerly wind at the low-level reached the highlands of Gifu prefecture. In the vertical cross-section along A-A' (Fig. 4.6b), the high EPT air reached the highlands (black dotted rectangle in Fig. 4.6b) and was lifted by the topography. The EPT decreased on the lee side of the highlands (red dotted rectangle in Fig. 4.6b). In the CNTL2,

the LCL and LFC of an air parcel averaged from the surface to 500-m height being lifted adiabatically were low levels of 963 hPa (approximately 406 m in altitude) and 956 hPa (approximately 470 m in altitude) at 2300 UTC 6 July 2018, respectively. The vertical profile averaged within the blue rectangle in Fig. 4.6a was used to calculate the LCL and LFC. The result indicates that the orographic lifting of the highlands of Gifu prefecture may be effective for convective cell genesis.

Figure 4.7 shows back trajectories using Golding (1984) method originating from the windward side of the SLPS at 0200 UTC 7 July 2018. According to the back trajectory originating from about a height of 1 km (Fig. 4.7a), the air parcel in the windward side of the SLPS inflowed from the Pacific Ocean and trajectories are widespread from 134° E to 137° E. The air parcels along the eastern trajectories through Ise Bay are more humid than the western ones. This indicates that most water vapor in the lower layer flowed to the highlands through Ise Bay. On the other hand, the air parcels along the back trajectories originating from a height of 4 km (Fig. 4.7b) are advected northeastward by the southwesterly. Most of the air parcels reached the windward side of the SLPS with keeping their altitudes (Figs. 4.7c and d). As a result, the low-level atmosphere on the windward side of the SLPS was more humid than the middle-level. This may intensify the convective instability on the windward side of the SLPS (see Fig. 4.6b).

According to the result of the CNTL2, the low-level southerly transported the warm and humid air toward the Baiu front. It reached the highlands of Gifu prefecture and was lifted by the topography. Consequently, convective cells formed and were transported northeastward by the middle-level southwesterly. This process continued in the steady environment condition, and the SLPS was maintained in Gifu prefecture. The CNTL2 result indicates that the topography of the highlands of Gifu prefecture was an essential factor in this SLPS event.

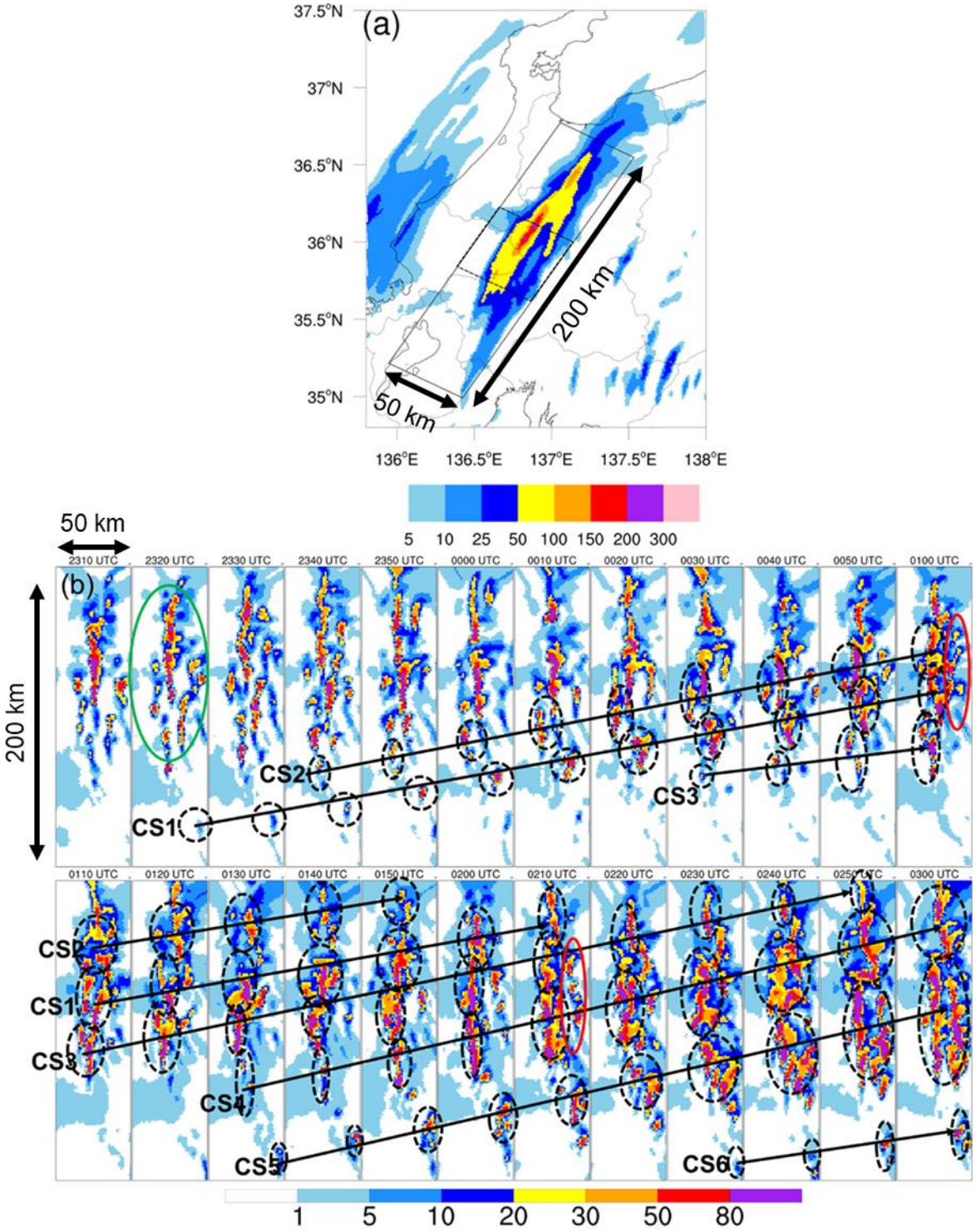

Fig. 4.4 (a) Total precipitation amount (mm) over Tokai district from 2300 UTC 6 July to 0300 UTC 7 July 2018, derived from the simulation results in CNTL2. (b) Rainfall rates (mm h^{-1}) in the solid rectangle in (a) from 2310 UTC 6 to 0300 UTC 7 July. CS1, CS2, CS3, CS4, CS5,

CS6, and CS7 indicate simulated convective clusters, and arrows show their movements. The dashed square is the region over which profiles of Fig. 4.9 are averaged.

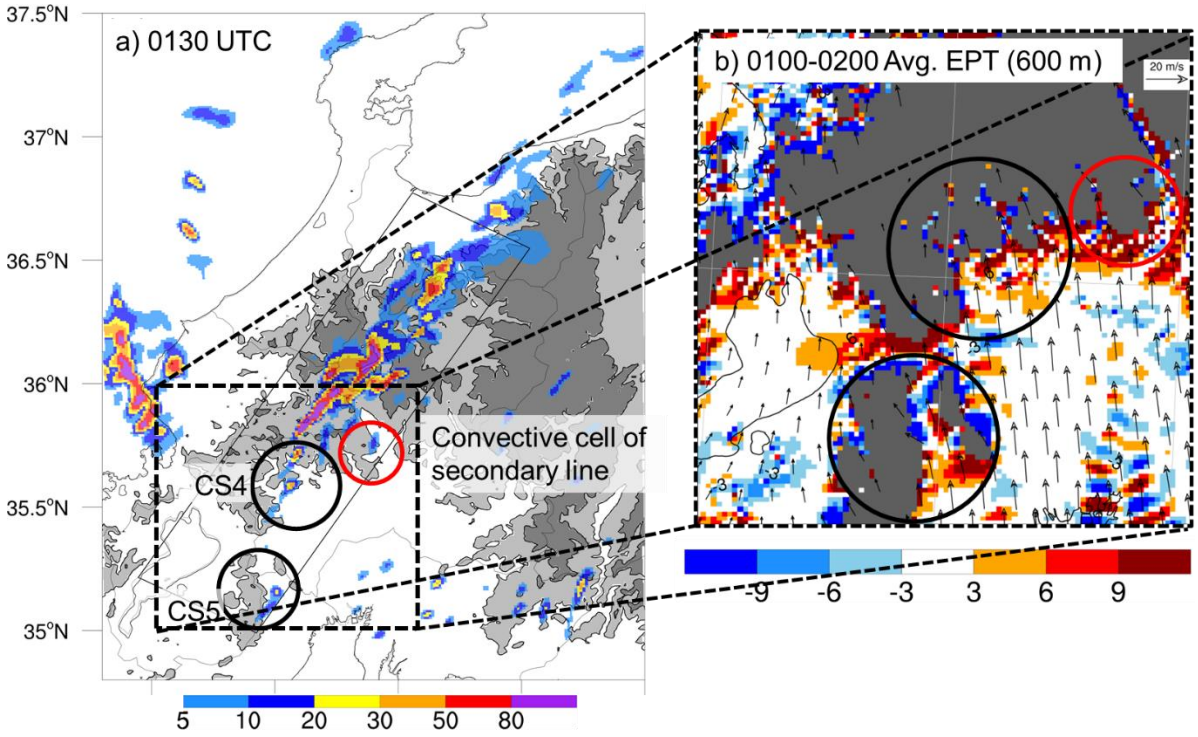

Fig. 4.5 (a) Rainfall rates (mm h^{-1}) at 0130 UTC 7 July 2018. The dashed square indicates the region over Fig. 4.5b. the shaded gray colors denote a height of 500 m and 1 km. (b) Averaged MFC (10^{-6} g $kg^{-1}s^{-1}$) distribution at a height of 600 m from 0100 UTC to 0200 UTC 7 July 2018. Arrows in (b) are the averaged horizontal winds. Areas under the ground are masked by gray color. Black and red circles indicate simulated convective cells of convective clusters and secondary convective line.

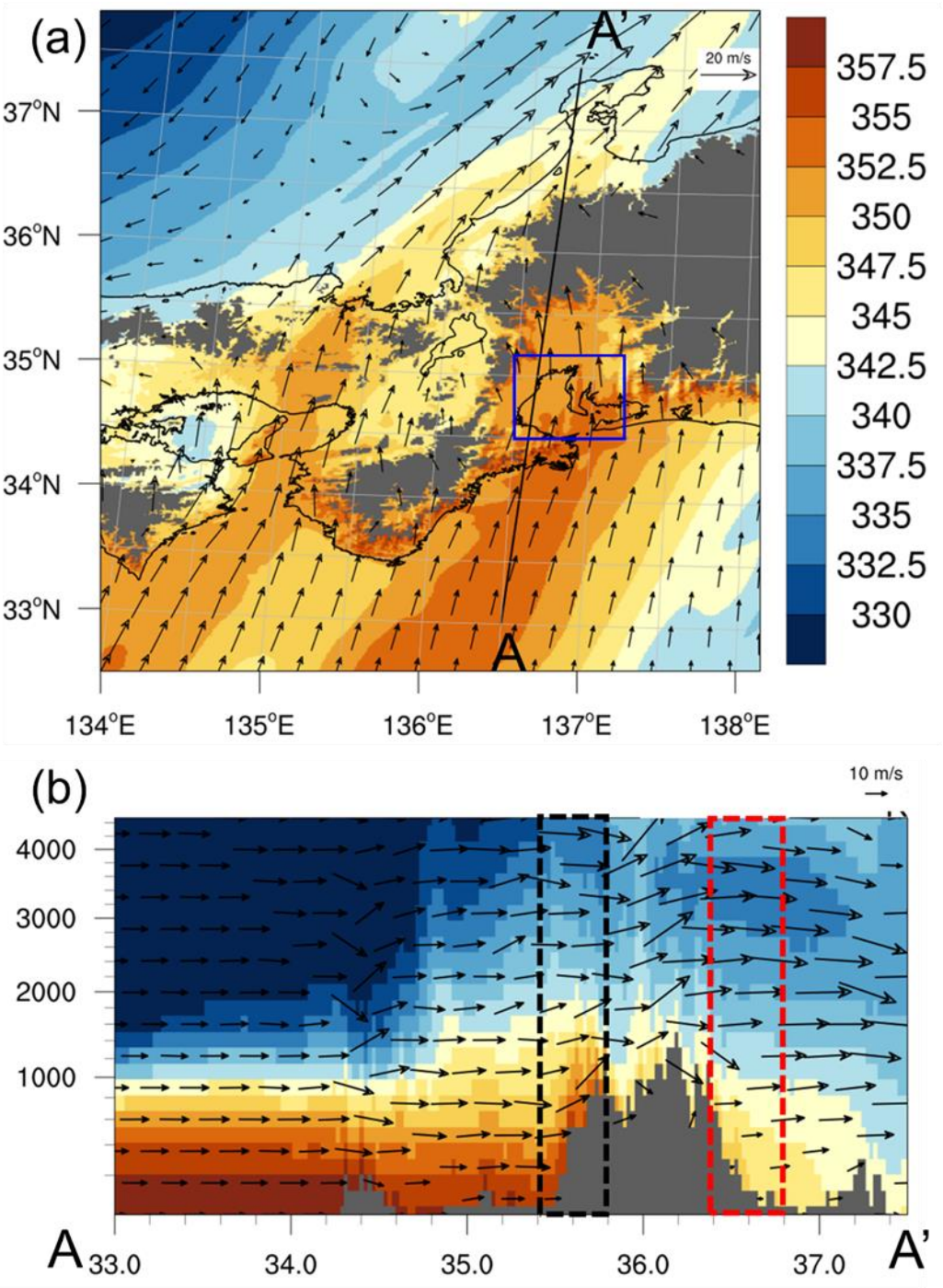

Fig. 4.6 (a) Averaged EPT (K) distribution at a height of 600 m from 2300 UTC 6 July to 0000 UTC 7 July 2018. Arrows in (a) are the averaged horizontal winds, and the blue rectangle is the region in which profiles are averaged for the calculations of the LCL and LFC. (b) Vertical

cross-sections along the line of AA'. Arrows are wind vectors in the vertical cross-section. For better visibility, the averaged vertical component of velocity was amplified 10 times. The scale of the velocity vector is shown above Fig. 4.6b. Areas under the ground are masked by gray color.

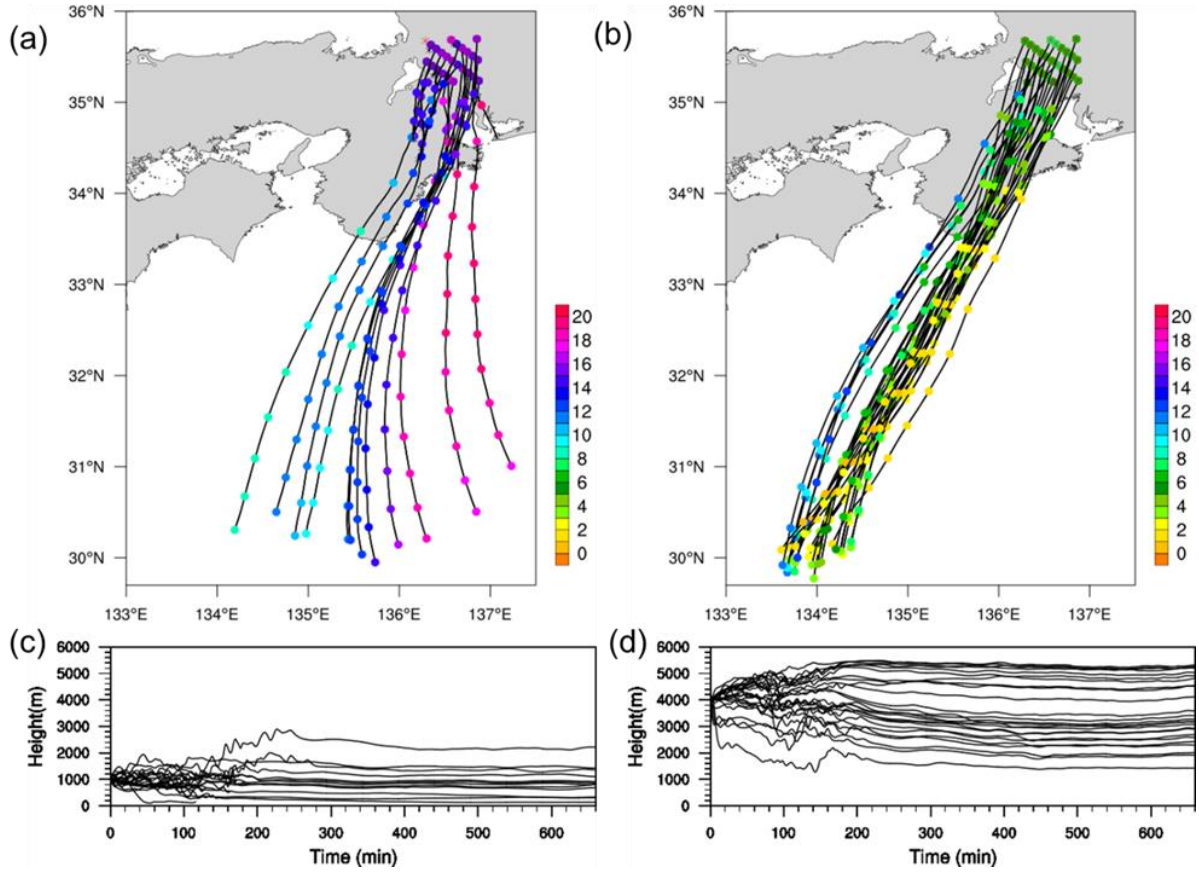

Fig. 4.7 Back trajectories and water vapor mixing ratio (g kg^{-1}) on the windward side of the SLPS at 0200 UTC 7 July 2018 at a height of (a) 1 km and (b) 4 km, derived from the simulation result of the CNTL. Dots along the trajectories in (a) and (b) are denoted at 1-hour intervals from 1500 UTC 6 to 0200 UTC 7 July 2018 and their colors denote water vapor mixing ratio. (c) and (d) show the heights of the trajectories in (a) and (b), respectively.

4.2.2 Sensitivity experiment

To investigate the role of the topography around the SLPS, two sensitivity experiments with modified topography: HT_LCL and HT_100M. The terrain height in the rectangle of Fig. 1.4c was lowered to the LCL (406 m in altitude) in the HT_LCL experiment and to 100 m in altitude in the HT_100M experiment. In HT_LCL, the SLPS was formed (Fig. 4.8a). On the other hand, in HT_100M, almost no SLPS appeared, small total precipitation amounts appeared on the windward side of SLPS (Fig. 4.8b). No secondary convective line appeared in HT_LCL and HT_100M experiments. In sensitivity experiments, the total precipitation amounts of the SLPS were significantly reduced, and the SLPS in HT_LCL slightly was shifted to the north in comparison to the CNTL2. In HT_100M, the total precipitation amount was distributed on the windward side of the observed SLPS (Fig. 4.8b). With regards to the time evolutions of convective cells of SLPS, convective cells in Gifu prefecture are weaker than those of CNTL2 in HT_LCL and no convective cells were found in HT_100M in the area of the observed SLPS (not shown). In addition, the lifetime of the generated convective cells on the Yoro mountains was shorter than that of the convective cells of SLPS in CNTL2.

In HT_LCL, the EPT vertical cross-section shows a weaker updraft and lifted EPT on the windward side of the highlands (black dotted rectangle in Fig. 4.9a) which is similar to CNTL2 (black dotted rectangle in Fig. 4.6b). However, In HT_100M, the high EPT on the windward side of the highlands (black dotted rectangle in Fig. 4.9b) was not lifted. The EPT on the lee

side (red dotted rectangle in Fig. 4.9) tended to be larger as the height of the highlands in Gifu prefecture was lowered. This indicates that warm and humid southerly at the low-level passed to the Sea of Japan. Consequently, precipitation amounts decreased over the highlands.

Table 4.2 summarizes the relationship between water vapor and total precipitation amounts in CNTL2 and sensitivity experiments. The windward side water vapor (WWV) and leeward side water vapor (LWV) values were averaged below 2 km in height within the black and red dotted rectangles in Figs. 4.6b and 4.9. Total precipitation amounts from 2300 UTC 6 to 0300 UTC 7 July were also averaged within the rectangle in Figs. 4.5a and 4.7. The WWV values of all the numerical experiments were almost the same to each other (15.8 and 15.9 g kg^{-1}). On the other hand, the LWV value became larger with lowering height of the terrain (13.5 in CNTL2 to 14.9 g kg^{-1} in HT_100M). The average total rainfall amount is larger with higher terrain height of the highlands in Gifu prefecture.

According to the results of sensitivity experiments, the highlands of Gifu prefecture played an important role to generate the SLPS and controlled the SLPS location and its total precipitation amount.

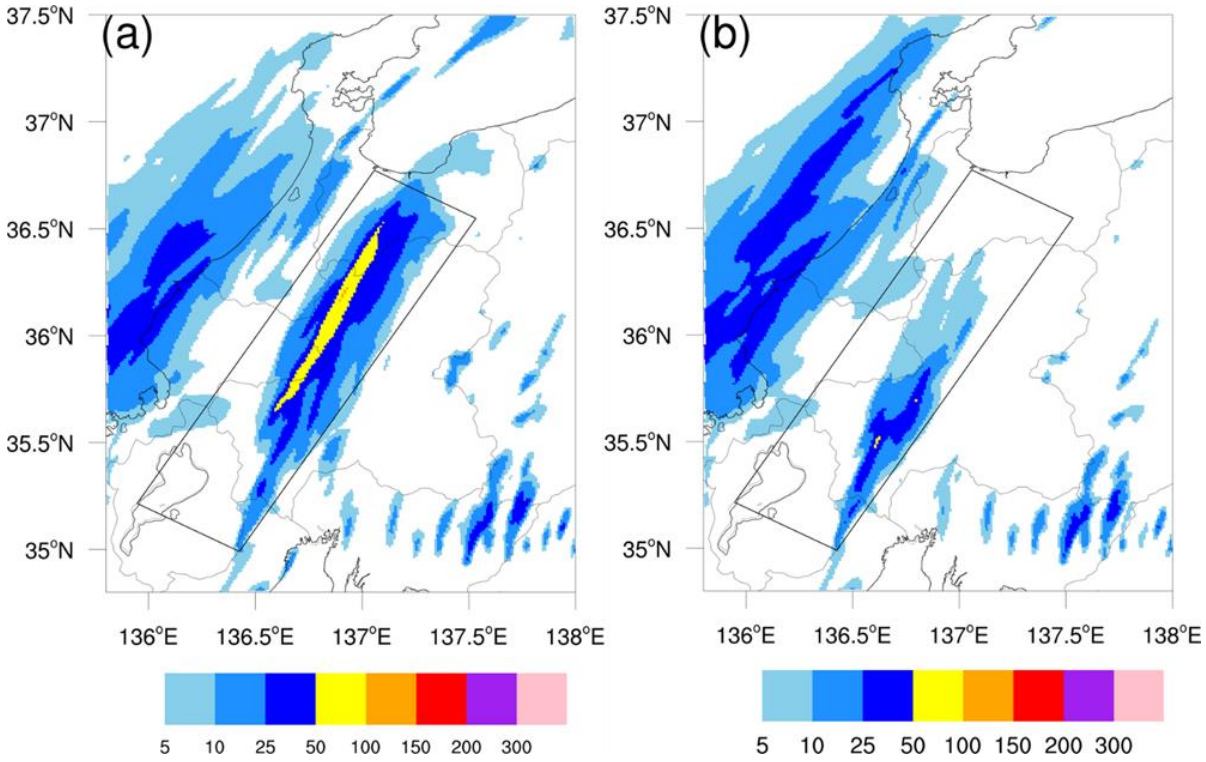

Fig. 4.8 Same as Fig. 4.4a, but for (a) HT_LCL and (b) HT_100M.

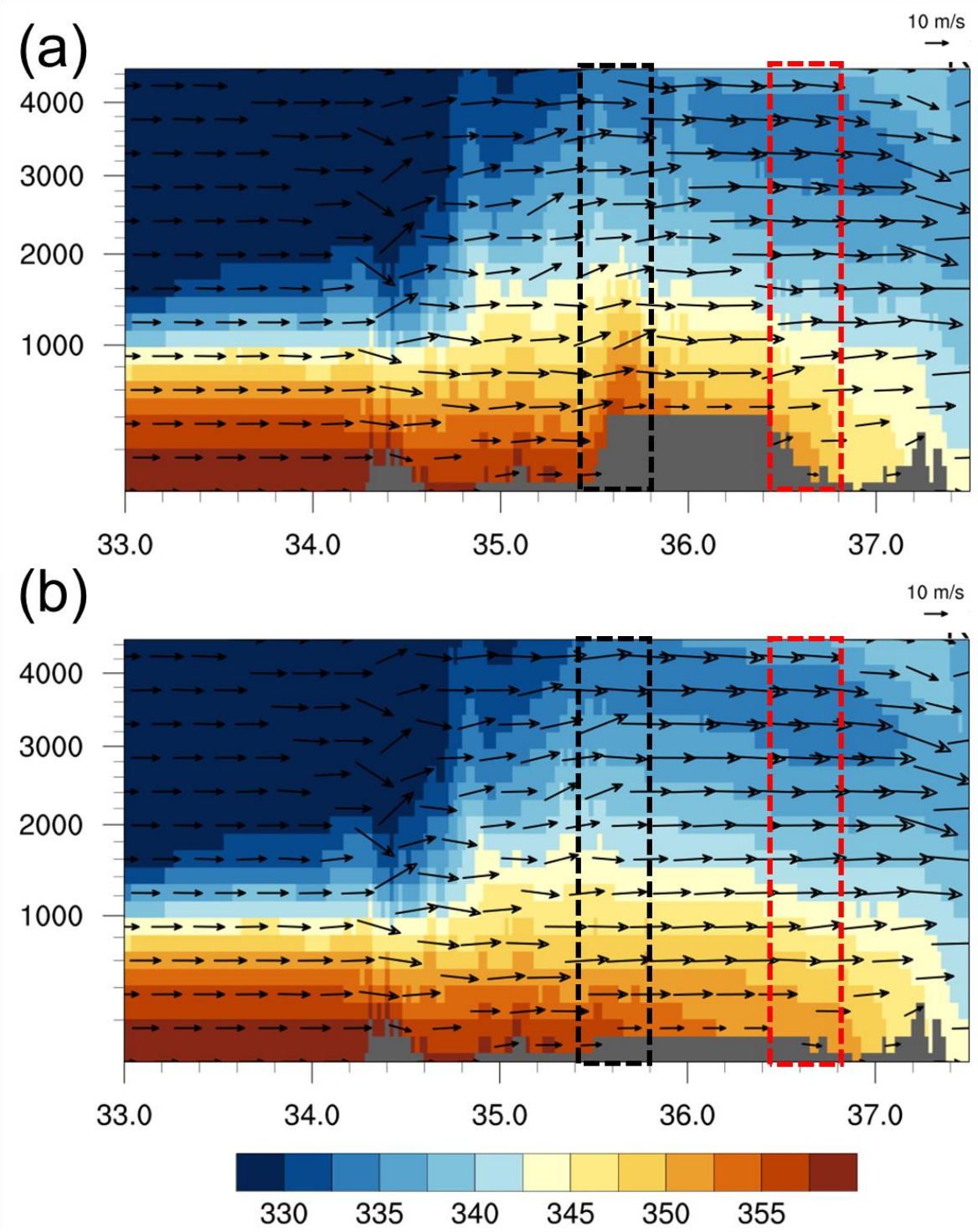

Fig. 4.9 Same as Fig. 4.6b, but for averaged (a) HT_LCL and (b) HT_100M from 2300 UTC 6 July to 0000 UTC 7 July 2018.

Table 4.2 Windward side water vapor (WWV) and leeward side water vapor (LWV) averaged from 2300 UTC 6 to 0000 UTC 7 July and averaged within the dashed rectangle in Figs. 4.6b and 4.9 below 2-km height, and total precipitation amounts averaged within the rectangles in Figs. 4.4a and 4.8 for CNTL2 and sensitivity experiments (HT_LCL and HT_100M).

	CNTL2	HT_LCL	HT_100M
WWV (g kg^{-1})	15.8	15.8	15.8
LWV (g kg^{-1})	13.5	14.2	14.9
Averaged total precipitation amounts (mm)	25.9	14.6	5.8

4.3 Discussion

On the basis of the observation and numerical experiments, this study investigated the formation and rainfall enhancement process of the SLPS that occurred on 7 July 2018 in Gifu prefecture. According to observation, the humid low-level southerly flowed into the inland region and convective cells can easily form by weak forcing. This indicates that the lifting by the terrain can easily generate convective cells.

Figure 4.10 shows the vertical profiles in the vicinity of the SLPS for each experiment. The values were averaged within the dashed square in Fig. 4.4a from 2300 UTC 6 to 0000 UTC 7 July. The vertical profiles of temperature (Fig. 4.10a) and water vapor mixing ratio (Fig. 4.10b) in the CNTL2, HT_LCL, and HT_100M were almost the same. This indicates that the thermodynamic conditions are almost the same in the CNTL2 and the sensitivity experiments. The wind speed and direction in the lower layer are different each other with the differences of height of the highlands (Figs. 4.10c and d). The wind speed below 500-m height became large with lowering height of terrain (11.8 m s^{-1} in CNTL2 to 19.2 m s^{-1} in HT_100M at 470 m).

The vertical wind speed is significantly larger in the CNTL2 than those of HT_LCL and HT_100M (Fig. 4.10e). In particular, the largest upward motion was located at a height of 2 km in the CNTL2. This suggests that the highlands lift the humid low-level air and convective cells develop. In this SLPS case, the highlands in Gifu prefecture played the role to trigger

convective cells of the SLPS. In addition, the highlands generated the secondary convective lines. They merged with the SLPS and enhanced the precipitation amount.

Figure 4.11 shows forward trajectories using Golding (1984) method originating from Ise Bay and its surrounding region at 2300 UTC 6 July 2018 at a height of 750 m for each experiment. According to the trajectory of the CNTL2 (Fig. 4.11a), most of the humid air with water vapor mixing ratio from over 16 g kg^{-1} traveled over the sea and the plain region, and was lifted by the topography of the highlands (1, 2, 4, 5, 6, and 9 lines in Fig. 4.10a). The rapidly lifted humid flow decreased the water vapor mixing ratio to below 6 g kg^{-1} and was moved northeastward by the southwesterly that was dominant in the upper level. In HT_LCL, some of trajectories were similar those of the CNTL2 (Fig. 4.11b). However, the other trajectories in HT_LCL and all of the trajectories in HT_100M (Fig. 4.11c) reached the Sea of Japan by the southerly without significant changes in trajectory height and water vapor mixing ratio. These results indicate the sufficient height of the highlands is necessary for the orographic enhancement process of the SLPS precipitation.

The vertical wind shear between the 500 m and 3 km in height were larger than 10 m s^{-1} in all numerical experiments (14.0 m s^{-1} in CNTL2, 11.7 m s^{-1} in HT_LCL, and 11.6 m s^{-1} in HT_100M). Previous studies found that the large vertical wind shear generated and maintained SLPS (Frank 1978; Bluestein and Jain 1985; Chen et al. 2015) and suggested that vertical wind shear is a key factor of SLPS formation (Seko et al. 1999; Kato 2020). The topography of the

highlands may contribute to increase the low-level vertical wind shear. The secondary convective lines on the southeast side of the SLPS were also generated by the highlands. These conditions were maintained by stagnated Baiu front. Consequently, in this SLPS case, the total precipitation amount was enhanced by the highlands in Gifu prefecture.

Previous SLPS in Tokai districts studies proposed that the key topography on windward side in SLPS of orography effect were Yoro mountains with Ibuki-Suzuka mountains (Fig. 1.4c) and Kii peninsula (34° N, 136° E) (Kato 2002; Moritomi et al. 2012). In this study, convective cells of SLPS were generated along two convergence zones on windward side (southwestern side) of SLPS (Fig. 4.5). In HT_100M, the convective cells were generated near Yoro-mountains. However, these convective cells did not form SLPS (Fig. 4.8b). It indicates that the highlands lifted an unstable atmosphere at low-level with inflowed humid southerly. Consequently, the highlands play the role not only the trigger of convective cells but also enhancing rainfall and extending the lifetime of convective cells.

The highlands in Gifu prefecture played two roles for the SLPS; the trigger and rainfall enhancement of convective cells composing the SLPS. The highlands in Gifu prefecture also caused the secondary convective lines which were merged with the SLPS. As a result, the total precipitation amount of the SLPS increased.

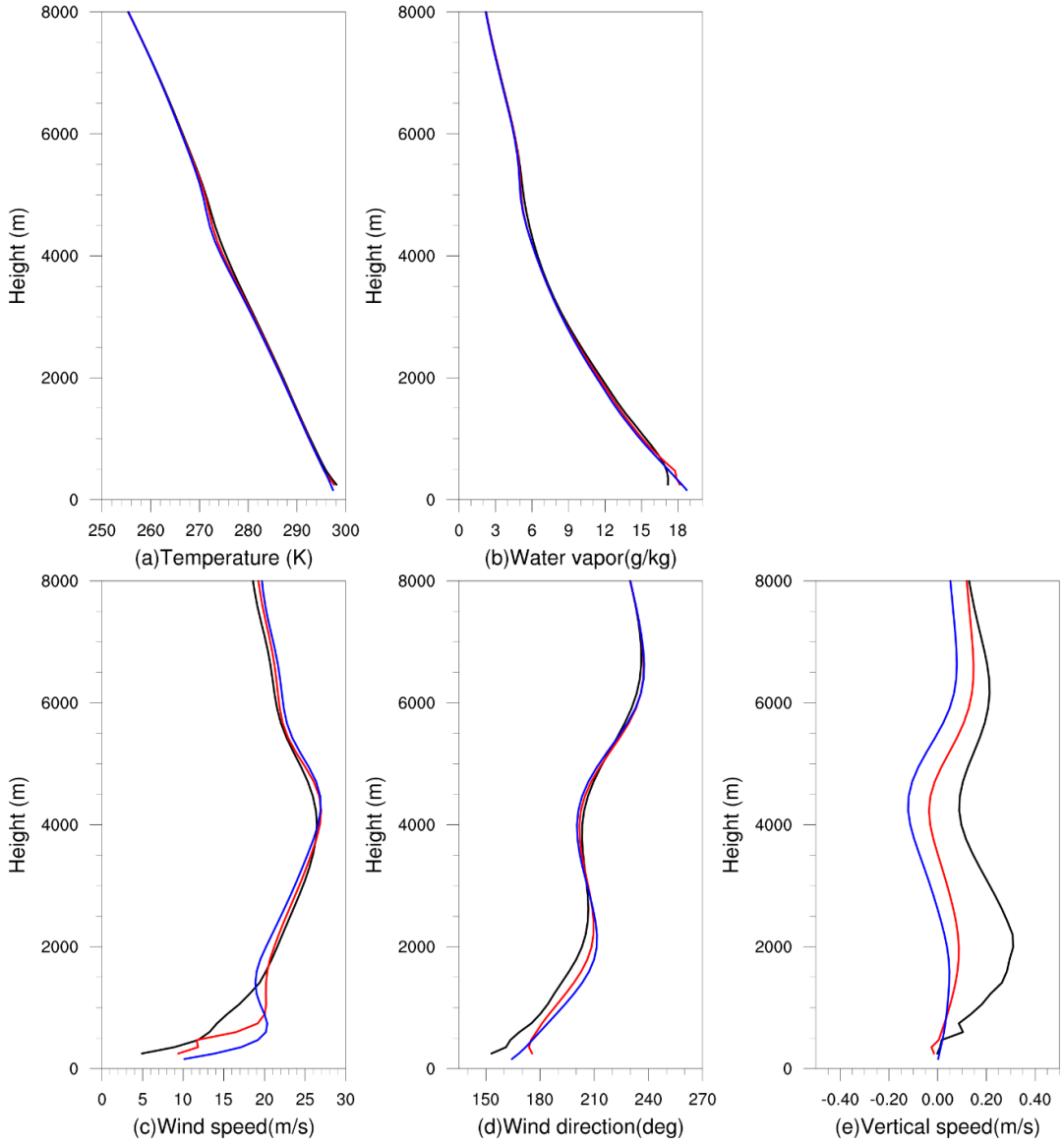

Fig. 4.10 The averaged vertical profiles of (a) temperature (K), (b) water vapor mixing ratio (g kg^{-1}), (c) wind speed (m s^{-1}), (d) wind direction (°), and (e) vertical speed (m s^{-1}). The black, red, and blue lines indicate CNTL2, HT_LCL, and HT_100M, respectively. The average was taken within the square of 50 × 50 km in Fig. 4.4a from 2300 UTC 6 July to 0000 UTC 7 July 2018.

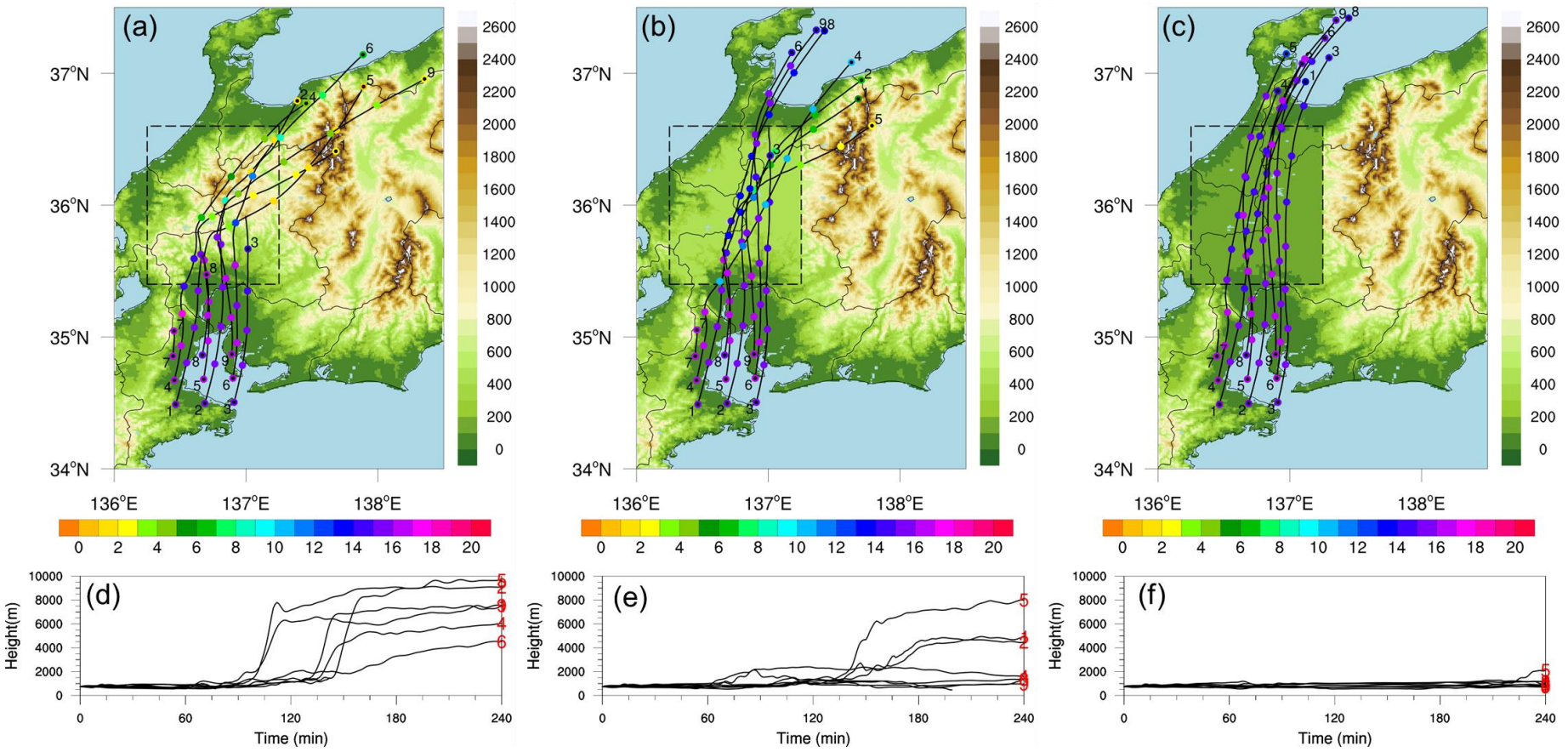

Fig. 4.11 Forward trajectories originating from Ise Bay and its surrounding region started at 2300 UTC 6 July 2018 at a height of 750 m for (a) CNTL, (b) HT_LCL, and (c) HT_100M, respectively. Dots along trajectories in (a), (b), and (c) are denoted at 30-min intervals from 2300 UTC

4 6 July to 0300 UTC 7 July 2018. The colors of dots indicate the water vapor mixing ratio (g kg^{-1}) of air parcels. Heights of trajectories are

5 shown in (d) CNTL, (e) HT_LCL, and (f) HT_100M. The dashed rectangle indicates where the topography is modified in the HT_LCL and

6 HT_100M experiments.

5. Summary

SLPSs prediction is difficult because they have complex mechanisms. For enhancement of prediction of SLPSs, the formation mechanism of SLPSs must be clarified and their conceptual model should be established. In this study, two SLPS cases were studied: 1 September 2015 over the Kinki district and 7 July 2018 over highlands in the Tokai district, respectively. To study the formation mechanisms of the SLPS, this study conducted observational data analysis and numerical experiments. In the Kinki district of Case1, the SLPS formation mechanism by orographic effect has been often reported. On the other hand, during Case2 event, the environmental conditions can easily form SLPS in the area.

In 1 September 2015, the upper-air sounding observed the upstream environment of the SLPS area showed that CAPE and LFC were respectively large and low, meaning that the SLPS formed in an unstable atmosphere. The wind direction at middle levels almost corresponded with the SLPS orientation. High- and low-pressure systems were located to the south and north of the Kinki district, respectively. Consequently, the strong southwesterly was present in the middle layer over the Kinki district. Unlike previous studies, a large-scale frontal system such as a cold front or a stationary front, was not observed in the Kinki district. From the numerical experiments, this study found that the SLPS was formed by the low-level convergence of the westerly with the warm and humid south-southwesterly in the Kinki district.

New cells successively formed over the north of Awaji Island were traveled by the middle-level southwesterly, and consequently the SLPS formed in the Kinki district (Fig. 5.1).

The sensitivity experiments for the orography showed that Mount Rokko and Awaji Island were not essential for the SLPS formation, although they modulated the location of the SLPS. From the sensitivity experiments for the initial time, this study found that one of the essential factors for the SLPS formation was the abundant supply of water vapor transported by the south-southwesterly through the Kii Channel. This south-southwesterly reached Osaka Bay, and converged with the westerly associated with the extratropical cyclone.

In addition, the sensitivity experiment for Shikoku Island showed that the topography of Shikoku Island dammed the south-southwesterly, and consequently the location and precipitation amounts of the SLPS were modulated. The SLPS formation mechanisms on 1 September 2015 are summarized as follows. First, a low-level convergence zone formed between the westerly and the warm and humid south-southwesterly in the Kinki district. The south-southwesterly flowed along the edge of the Pacific high-pressure system through the Kii Channel. On the other hand, the westerly region was found associated with an extratropical cyclone located in the north of Japan. Second, convective cells successively formed in the convergence zone where the atmosphere was conditionally unstable due to the inflow of the low-level warm and humid south-southwesterly. Third, the successively formed convective cells were traveled to the downstream (northeast) by the middle-level southwesterly. The

second and third processes were repeated, and consequently the SLPS formed in the Kinki district.

During Heavy Rainfall Event Japan in 2018 (HREJ2018), a heavy rainfall event occurred over the highlands of Gifu prefecture with a total precipitation amount of 1214. 5 mm and the precipitation amount recorded from 6 to 7 July 2018 was roughly a half of the total of the HREJ2018 period. There were two intense rainfall periods over 80 mm in three-hour rainfall amount: HR1 (from 0700 UTC to 1100 UTC 6 July 2018) and HR2 (from 2300 UTC 6 July to 0300 UTC 7 July 2018). During the period of HR2, Hirugano AMeDAS in Gifu prefecture recorded 131.5 mm for four hours. This study performed a simulation experiment (CNTL2) and two sensitivity experiments on the orography. In the CNTL2 experiment, the SLPS in HR2 was formed owing to the inflow of the warm and humid southerly to the south of the Baiu front.

The inflow air was lifted by the topography of the highlands and reached the LFC. This resulted in the convective cell formation. The convective cells were moved northeastward by the middle-level southwesterly and they were organized into the SLPS. This process continued due to the stagnation of the Baiu front (Fig. 5.2). In sensitivity experiments for the orographic effect around SLPS, the terrain height of the highlands was reduced to the LCL height of the 406-m (HT_LCL) and to 100-m height (HT_100M). In these experiments, the warm and humid southerly at the low-level passed through the highland region to the Sea of Japan without a significant upward motion because the lowered topography is ineffective to lift the humid air.

As a result, the total precipitation amount of the SLPS and the rainfall intensity of the convective cells were significantly reduced than those of the CNTL2. Furthermore, the topography generated the secondary convective lines. The successive formations of convective cells and the secondary convective lines resulted in the rainfall enhancement of the SLPS. The result indicates that the highlands of Gifu prefecture played an important role in the formation and rainfall enhancement of the SLPS.

In summary of this study, the SLPS case over the highlands of Gifu prefecture was caused not only by low-level humid inflow by stagnant Baiu front but also by the terrain. They determined the formation and location, and enhanced rainfall. Case1 (1 September 2015 over the Kinki district) showed a different mechanism from the SLPS formation mechanism indicated by previous studies. In addition, the topographic effect is different by region and seasons and causes differences for SLPS cases.

The study of SLPS cases with these complex characteristics is expected to help construct a conceptual model for predicting each region's SLPS during the warm season in the future. However, for a more understanding of the SLPSs rainfall enhancement process, analyses of convective cell three-dimensional dynamics are required.

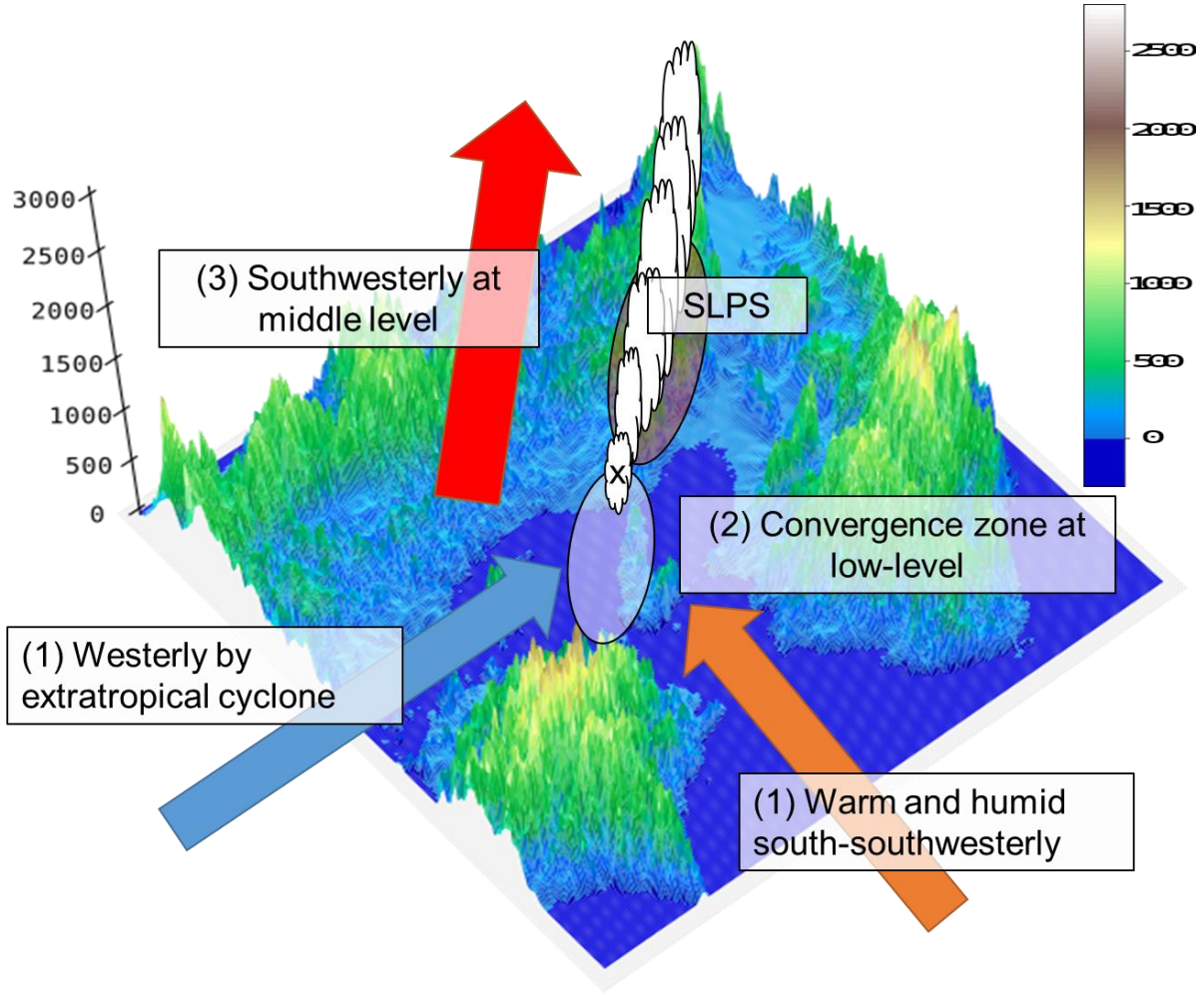

Fig. 5.1 Schematic of SLPS formation mechanism on 1 September 2015.

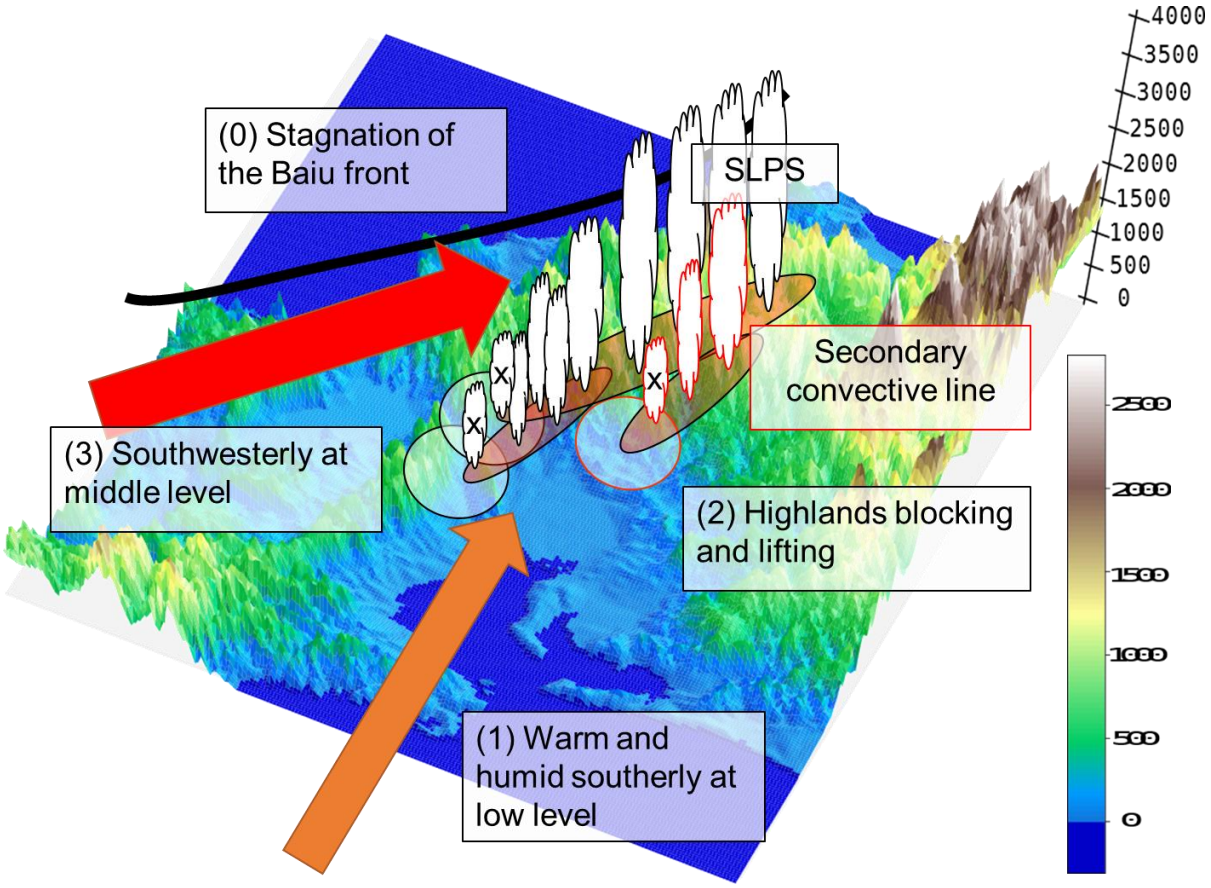

Fig. 5.2 Schematic of SLPS formation mechanism on 7 July 2018.

Acknowledgment

I would like to thank Prof. Kazuhisa Tsuboki, ISEE, Nagoya University. As my teacher and mentor, he has taught me more than I could ever give him credit for here. He has shown me, by his example, what a good scientist (and person) should be. I would also like to my secondary supervisors thank Prof. Hiroshi Uyeda, an emeritus professor of Nagoya University, Prof. Nobuhiro Takahashi, and Prof. Taro Shinoda, ISEE, Nagoya University for their advice and feedback. Their varied perspectives have helped me to strengthen my work. I would like to thank Dr. Sachie Kanada, who has been an invaluable mentor. Her enduring encouragement and her practical advice have been an inestimable source of support for me during this process. I would like to thank Dr. Mayumi Yoshioka of Earth Observation Research and application Center, Japan Aerospace Exploration Agency, Ms. Yukie Moroda, and Mr. Masaya Kato of ISEE, Nagoya University for their assistance with the observation and numerical experiments analysis. I would like to thank all of the students and mentors who gave their time and provided me with insight into their experience with the laboratory of Meteorology, ISEE, Nagoya University. Finally, I would like to thank my parents and older sister's family in Korea.

All the computations of the numerical simulations and experiments were performed on the supercomputer of the Information Technology Center, Nagoya University. The observational data and initial condition data of the numerical experiments were provided by the Japan Meteorological Agency. The skew T-log P in the study is the data from Wyoming University

(http://weather.uwyo.edu/upperair/sounding.html). This work was jointly supported by KAKENHI Grants 15H05765 and 16H06311, and the Virtual Laboratory for the Earth's Climate Diagnostics program. NCAR Command Language (NCL) was used to draw the figures.

References

Banacos P.C. and D.M. Schultz, 2005: The use of moisture flux convergence in forecasting convective initiation: Historical and operational perspectives. *Wea. Forecasting*, **20**, 351-366.

Bluestein H. B. and M.H. Jain, 1985: Formation of mesoscale lines of precipitation: Severe squall lines in Oklahoma during the spring. *J. Atmos. Sci.*, **42**, 1711-1732.

Bolton D., 1980: The Computation of Equivalent Potential Temperature. *Mon. Wea. Rev.*, **108**, 1046-1053.

Chen, Q., J. Fan, S. Hagos, W. I. Gustafson Jr., and L. K. Berg 2015: Roles of wind shear at different vertical levels: Cloud system organization and properties. *J. Geophys. Res. Atmos.*, **120**, 6551–6574.

Cotton, W. R., G. J. Tripoli, R. M. Rauber, and E. A. Mulvihill, 1986: Numerical simulation of the effects of varying ice crystal nucleation rates and aggregation processes on orographic snowfall. *J. Climate Appl. Meteor.*, **25**, 1658-1680.

Deardorff, J. W., 1980: Stratocumulus-capped mixed layers derived from a three-dimensional model. *Bound.-Layer Meteor.*, **18**, 495-527.

Frank W. M., 1978: The life cycles of GATE convective systems. *J. Atmos. Sci.*, **35**, 1256-1264.

Gallus, W. A., N. A. Snook, and E. V. Johnson, 2008: Spring and summer severe weather reports over the Midwest as a function of convective mode: A preliminary study. *Wea. Forecasting*, **23**, 101-113.

Golding, B., 1984: A study of the structure of midlatitude depressions in a numerical model using trajectory techniques. I: Development of ideal baroclinic waves in dry and moist atmosphere. *Quart. J. Roy. Meteor. Soc.*, **110**, 847-879.

Higashi K., Y. Kiyohara and M. Yamanaka, 2010: Multiscale features of line-shaped precipitation system generation in central Japan during late Baiu season. *J. Meteor. Soc. Japan*, **88**, 909-930.

Hirockawa, Y., T. Kato, H. Tsuguti, and N. Seino, 2020: Identification and classification of heavy rainfall areas and their characteristic features in Japan. *J. Meteor. Soc. Japan*, **98**, 835-857.

Houze, Jr., R. A., 1993: Cloud Dynamics. *International geophysics series*, **104**, *Academic Press*, 496 pp.

Houze, Jr., R. A., 2004: Mesoscale convective systems, *Rev. Geophys.*, **42**, RG4003, doi:10.1029/2004RG000150.

Ikawa, M., and K. Saito, 1991: Description of a nonhydrostatic model developed at the Forecast Research Department of the MRI. MRI Tech. Rep. 28, 238 pp.

Ishihara M. and K. Takara, 2018: The rainstorm generated around Uji, Kyoto on 13-14 August 2012 Part I: Mesoscale analysis of the convective line systems causing heavy rainfall. *Tenki*, **65**, 5-23 (in Japanese).

Japan Meteorological Agency (JMA), 2013: Outline of the operational numerical weather prediction at the Japan Meteorological Agency. [Available at http://www.jma.go.jp/jma/jma-eng/jma-center/nwp/outline2013-nwp/index.htm]

Japan Meteorological Agency (JMA), 2018: primary factors behind the Heavy Rain Event of July 2018 and the subsequent heatwave in Japan from mid-July onward. Press Release of Tokyo Climate Center

[Available at https://ds.data.jma.go.jp/tcc/tcc/news/press_20180822.pdf]

Kato, T. and H. Goda, 2001: Formation and maintenance processes of a stationary band-shaped heavy rainfall observed in Niigata on 4 August 1998. *J. Meteor. Soc. Japan*, **79**, 899-924.

Kato, T., 2002: Modelling and forecasts of heavy rainfall Approach with numerical experiments. *Tenki*, **49**, 626–634 (in Japanese).

Kato T., 2006: Structure of the band-shaped precipitation system inducing the heavy rainfall observed over northern Kyushu, Japan on 29 June 1999. *J. Meteor. Soc. Japan*, **84**, 129-153.

Kato T., 2020: Quasi-stationary band-shaped precipitation systems, named as “senjo-kousuitai”, causing localized heavy rainfall in Japan. *J. Meteor. Soc. Japan*, **98**, doi: 10.2151/jmsj.2020-029.

Kawano T. and R. Kawamura, 2020: Genesis and Maintenance Processes of a Quasi-Stationary Convective Band that Produced Record-Breaking Precipitation in Northern Kyushu, Japan on 5 July 2017. *J. Meteor. Soc. Japan*, **98**, doi: 10.2151/jmsj.2020-033.

Kurihara K., T. Kanamori and H. Seko, 2009: Band-shaped precipitation system observed in Hiroshima on 18 July 2003 ―Airflow structure and the effects of terrain and middle-level dry air analyzed by JMANHM―. *Tenki*, **56**, 613–626 (in Japanese).

Louis, J. F., M. Tiedtke, and J. F. Geleyn, 1981: A short history of the operational PBL parameterization at ECMWF. *Workshop on Planetary Boundary Layer Parameterization*, 25-27 November 1981, Reading, UK, 59-79.

Lin, Y.L., R.D. Farley, and H.D. Orville, 1983: Bulk parameterization of the snow field in a cloud model. *J. Appl. Meteor.*, **22**, 1065-1092.

Lin, Y., 2007: Dynamics of orographic precipitation. In Mesoscale Dynamics. *Cambridge: Cambridge University Press*. doi:10.1017/CBO9780511619649.012

Meteorological Research Institute (MRI), 2010: Studies on formation process of line-shaped rainfall systems and predictability of rainfall intensity and moving speed, *Technical Report of the MRI*, **61**, 159 pp (in Japanese).

Murakami, M., 1990: Numerical modeling of dynamical and microphysical evolution of an isolated convective cloud---The 19 July 1981 CCOPE cloud. *J. Meteor. Soc. Japan*, **68**, 107-128.

Murakami, M., T. L. Clark, and W. D. Hall, 1994: Numerical simulations of convective snow clouds over the Sea of Japan: Two-dimensional simulation of mixed layer development and convective snow cloud formation. *J. Meteor. Soc. Japan*, **72**, 43-62.

Morotomi, K., T. Shinoda, Y. Shusse, T. Kouketsu, T. Ohigashi, K. Tsuboki, H. Uyeda and I. Tamagawa, 2012: Maintenance Mechanisms of a Precipitation Band Formed along the Ibuki-Suzuka Mountains on September 2-3, 2008. *J. Meteor. Soc. Japan*, **90**, 737-753.

Ogura Y., 1991: Analysis and mechanism of intense precipitation. *Tenki*, **38**, 276–288 (in Japanese).

Parker M. D. and R. H. Johnson, 2000: Organizational modes of midlatitude mesoscale convective systems. *Mon. Wea. Rev.*, **128**, 3413-3436.

Schultz D.M., P. N. Schumacher, and C. A. Doswell, 2000: The intricacies of instabilities. *Mon. Wea. Rev.*, **128**, 4143-4148.

Schumacher and Johnson, 2005: Organization and environmental properties of extreme-rain-producing mesoscale convective systems. *Mon. Wea. Rev.*, **133**, 961–976.

Seko, H., T. Kato, K. Saito, M. Yoshizaki, K. Kusunoki, M.Maki, and Members of Tsukuba Area Precipitation studies, 1999: Analytical and numerical studies of a quasi-stationary precipitation band observed over the Kanto area associated with Typhoon 9426 (Orchid). *J. Meteor. Soc. Japan*, **77**, 929-948.

Seko, H., and H. Nakamura, 2003: Numerical study of the shapes and maintenance mechanisms of meso-β scale line-shaped precipitation system in the middle-latitudes. *CAS/JSC WGNE Research Activities in Atmospheric and Oceanic Modelling*, **33**, 5.30–5.31.

Seko, H., Y. Kumahara, and K. Saito, 2006: Line-shaped convective band developed over the Osaka Plain. *CAS/JSC WGNE Research Activities in Atmospheric and Oceanic Modelling*, **36**, 5.53–5.54.

Seko, H., 2010: Study of the shapes and maintenance mechanisms of meso-β scale line-shaped precipitation systems in the middle-latitudes. *J. Meteor. Res.*, **62**, 1-74 (in Japanese).

Smagorinsky, J., 1963: General Circulation Experiments with the Primitive Equation I the Basic Experiment. *Mon. Wea. Rev.*, **91**, 99-164.

Sueki, K., and Y. Kajikawa, 2019: Different precipitation systems between Hiroshima and Keihanshin during extreme rainfall event in western Japan in July 2018. *J. Meteor. Soc. Japan*, **97**, 1221-1232.

Sun, J. and T.Y. Lee, 2002: A numerical study of an intense quasi-stationary convection band over the Korean Peninsula. *J. Meteor. Soc. Japan*, **80(5)**, 1221-1245.

Takasaki Y., M. Yoshizaki, A. Suzuki-Parker, and Y. Watarai, 2019: Sensitivity of quasi-stationary band-shaped precipitation system to topography: A case study for 28 August 2008 Okazaki heavy rainfall event. *J. Meteor. Soc. Japan*, **97**, 453-466

Tsuboki K. and A. Sakakibara, 2002: Large-scale parallel computing of Cloud Resolving Storm Simulator. *in High Performance Computing*, *Springer*, *New York*, 243–259.

Tsuboki K. and A. Sakakibara, 2007: Numerical prediction of high-impact weather systems. *The Textbook for Seventeenth IHP Training Course in 2007*, 281pp.

Tsuguti H. and T. Kato, 2014a: Objective extraction of heavy rainfall events and statistical analysis on their characteristic feature. *Tenki*, **61**, 455-469 (in Japanese).

Tsuguti, H., and T. Kato, 2014b: Contributing factors of the heavy rainfall event as Amami-Oshima Island, Japan, on 20 October 2010. *J. Meteor. Soc. Japan*, **92**, 163–183.

Tsuguti H., 2016: Line-shaped precipitation system. *Tenki*, **63**, 727-729 (in Japanese).

Tsuguti H., 2019: Description of the Line-shaped Precipitation System Causing Heavy Rainfall. *J. Environ. Con. Eng*, **48**, 180-184 (in Japanese).

Unuma, T. and T. Takemi, 2016a: Characteristics and environmental conditions of quasi-stationary convective clusters during the warms eason in Japan, *Q. J. R. Meteorol. Soc.*, **142**, 1232–1249.

Unuma, T. and Takemi, T., 2016b: A role of environmental shear on the organization mode of quasi-stationary convective clusters during the Warm season in Japan. *SOLA*, **12**, 111-115.

Wang, S.-Y., and T.-C. Chen, 2008: Measuring East Asian summer monsoon rainfall contributions by different weather systems over Taiwan. *J. Appl. Meteor. Climatol.*, **47**, 2068–2080.

Yoshizaki, M., T. Kato, Y. Tanaka, H. Takayama, Y. Shoji, H. Seko, K. Manabe and Members of X-BAIU-98 Observation, 2000: Analytical and numerical study of the 26 June 1998 orographic rainband observed in western Kyushu, Japan. *J. Meteor. Soc. Japan*, **78**, 835-856.